Supporting Information for

Size-Discrimination for VOCs Utilizing Gallium Diiminate by Luminescent Chromism of CIE via Encapsulation-Triggered Crystal−Crystal Transition

Shunichiro Ito, Amane Hirose, Madoka Yamaguchi, Kazuo Tanaka and Yoshiki Chujo**

Department of Polymer Chemistry, Graduate School of Engineering, Kyoto University, Katsura, Nishikyo-ku, Kyoto 615-8510, Japan

Corresponding author E-mail: chujo@chujo.synchem.kyoto-u.ac.jp

Tel: (+81)-75-383-2604. Fax: (+81)-75-383-2605

Experimental Section

Measurements: ^{1}H (400 MHz) and ^{13}C (100 MHz) NMR spectra were recorded on JEOL JNM-EX400 spectrometers. In ^{1}H and ^{13}C NMR spectra, tetramethylsilane (TMS) was used as an internal standard in $CDCl_3$. UV−vis absorption spectra were recorded on a SHIMADZU UV–3600 spectrophotometer, and UV−vis diffuse reflection spectra were measured with integrating sphere attachment, ISR-3100, and barium sulfate white plate as a standard plate. Fluorescence emission spectra were measured with a HORIBA JOBIN YVON Fluoromax–4P spectrofluorometer, and photoluminescence quantum yields were calculated by integrating sphere method. Elemental analysis was performed at the Microanalytical Center of Kyoto University. Photoluminescence (PL) lifetimes were measured by a Horiba FluoreCube spectrofluorometer system and excitation was carried out at 375nm using UV diode laser (NanoLED 375 nm). Powder X-ray diffraction (XRD) patterns were taken by using CuKα radiation with a Rigaku Miniflex. For the Rietveld refinements, powder patterns were measured using Rigaku SmartLab. Elemental analysis was performed at the Microanalytical Center of Kyoto University. DSC thermograms were carried out on a SII DSC 6220 instrument. The sample on the sealing aluminum pan was heated at the rate of 10 °C/min under nitrogen flowing (20 mL/min).

Materials: Anhydrous gallium chloride (Tokyo Chemical, Co.) was used as received. Diethyl ether and triethylamine were purified using a two-column solid-state purification system (Glasscoutour System, Joerg Meyer, Irvine, CA).

Synthesis of 1: 1 was synthesized according to our previous work.[1]

Synthesis of 2: $GaCl_3$ (0.94 g, 5.3 mmol) in diethyl ether (20 mL) was added to the solution of **1** (0.50 g, 1.3 mmol) in toluene (30 mL) at room temperature under argon atmosphere. NEt_3 (0.54 g, 0.74 mL, 5.3 mmol) was added to the mixture solution. The color of the solution turned from dark orange to light yellow. The mixture solution was stirred at 100 °C for 15 h. after the solvent was removed by a rotary evaporator, the product was extracted by CH_2Cl_2 (10 mL). The filtrate was dropped into methanol (50 mL), leading to precipitating the desire compound. The solid collected by filtration was dried in vacuum

at 110 °C for 24 h to give pure **2** as a yellow crystal (0.61 g, 88%). ^{1}H NMR ($CDCl_3$): δ = 7.27−7.05 (20H, m), 5.45 (1H, =CH-, s) ppm. ^{13}C NMR ($CDCl_3$): δ = 170.63, 143.85, 138.03, 129.38, 128.87, 128.80, 128.11, 126.47, 126.15, 101.54 ppm. HRMS (ESI): Calcd for $[M+H]^+$, 513.0410; found, m/z 513.0407. Anal. Calcd for $C_{27}H_{21}Cl_2GaN_2$: C, 63.08; H, 4.12; N, 5.45. Found: C, 63.23; H, 4.20; N, 5.40.

Dispersion of gallium or boron complexes in PMMA films: The PMMA films including 1 wt% of gallium and boron diiminate complexes were prepared with a spin-coat method (1500 rpm) from 50 μL $CHCl_3$ solution (1.0×10^{-3} M of each complex and PMMA mixture). PMMA (nacalai tesque, inc., $M_n \approx$ 800,000) was used as received.

Condition of solvent vaporization: The prisitne samples of the gallium diiminate were left under organic solvent atmosphere at room temperature for 24 h using 17 types of organic solvents such as cyclohexane, acetone, toluene, benzene, THF, furan, pyridine, 1,4-dioxane, chlorobenzene, bromobenzene, iodobenzene, pentane, hexane, acetonitrile, methanol, diacetyl and dichloromethane. As a result, cyclohexane, acetone, toluene, benzene, THF, furan, pyridine and 1,4-dioxane were captured in the crystalline samples. On the other hand, chlorobenzene, bromobenzene, iodobenzene, pentane, hexane, acetonitrile, methanol, diacetyl and dichloromethane were not captured.

NMR Spectra

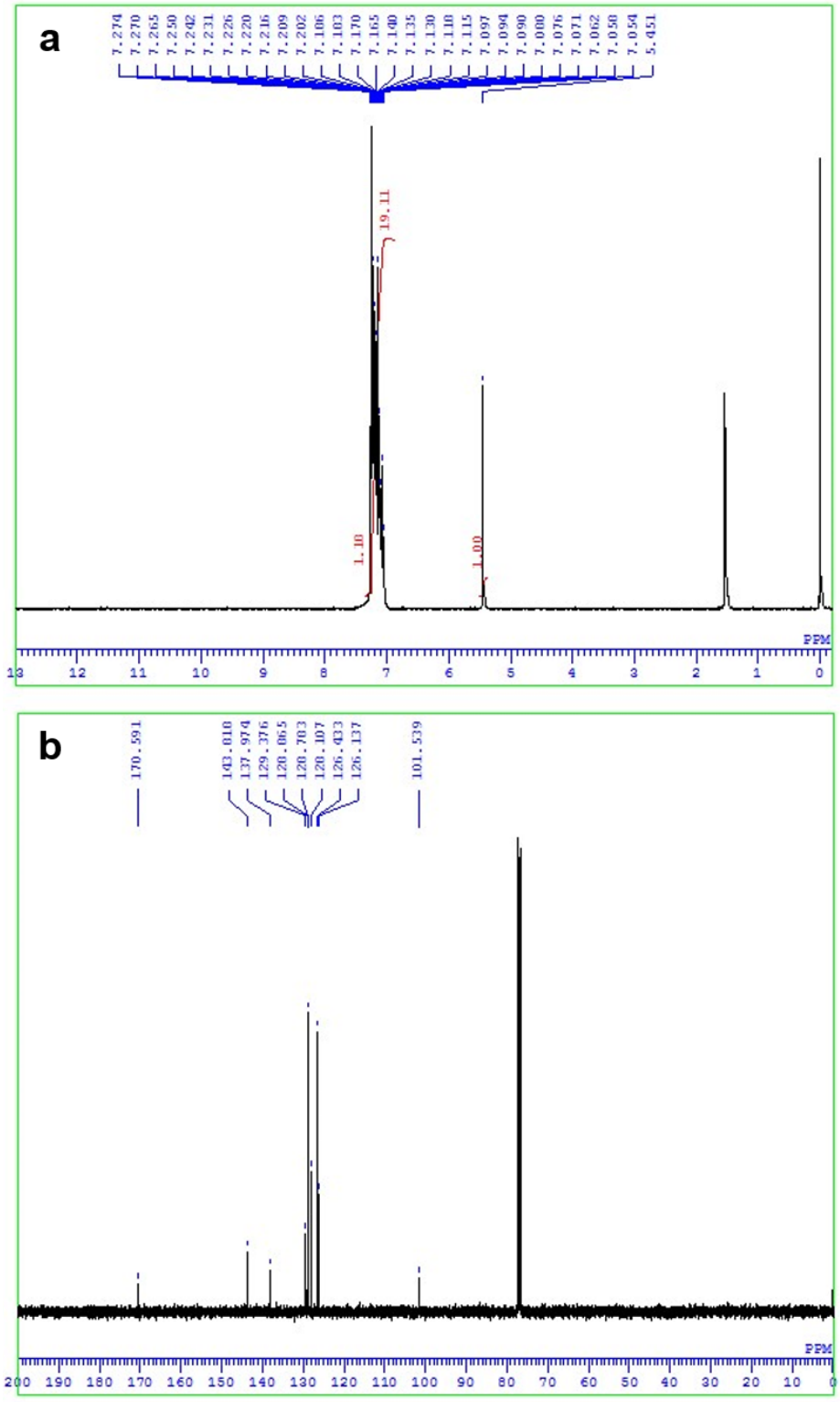

Figure S1. a) ^{1}H, b) ^{13}C NMR spectra of **2** in $CDCl_3$.

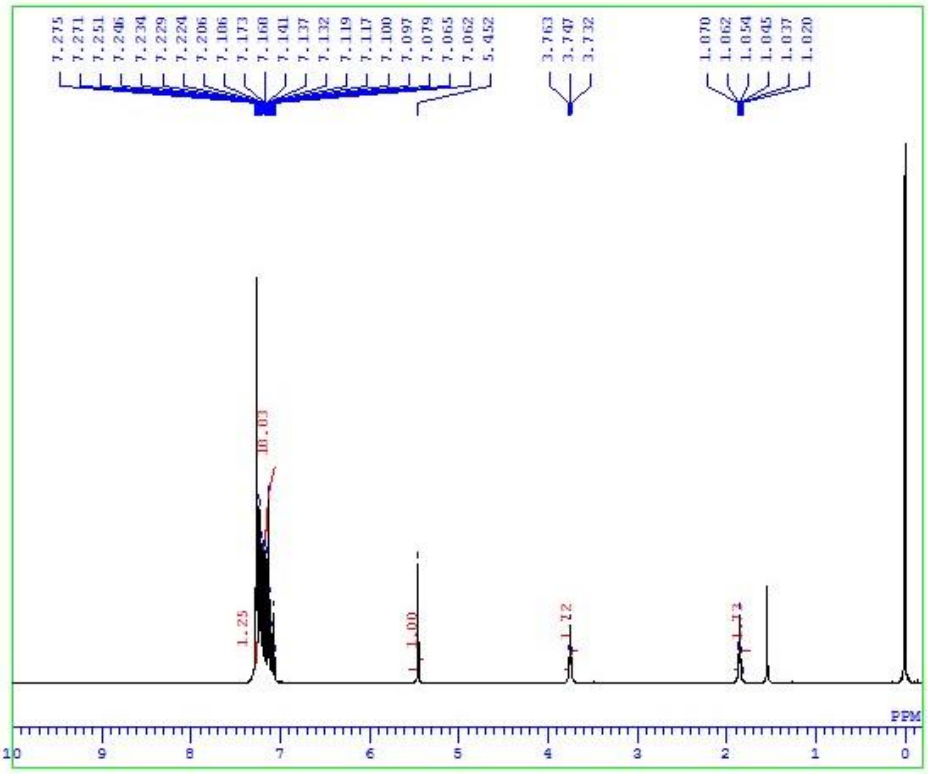

Figure S2. ^{1}H NMR spectrum of phase **G**.

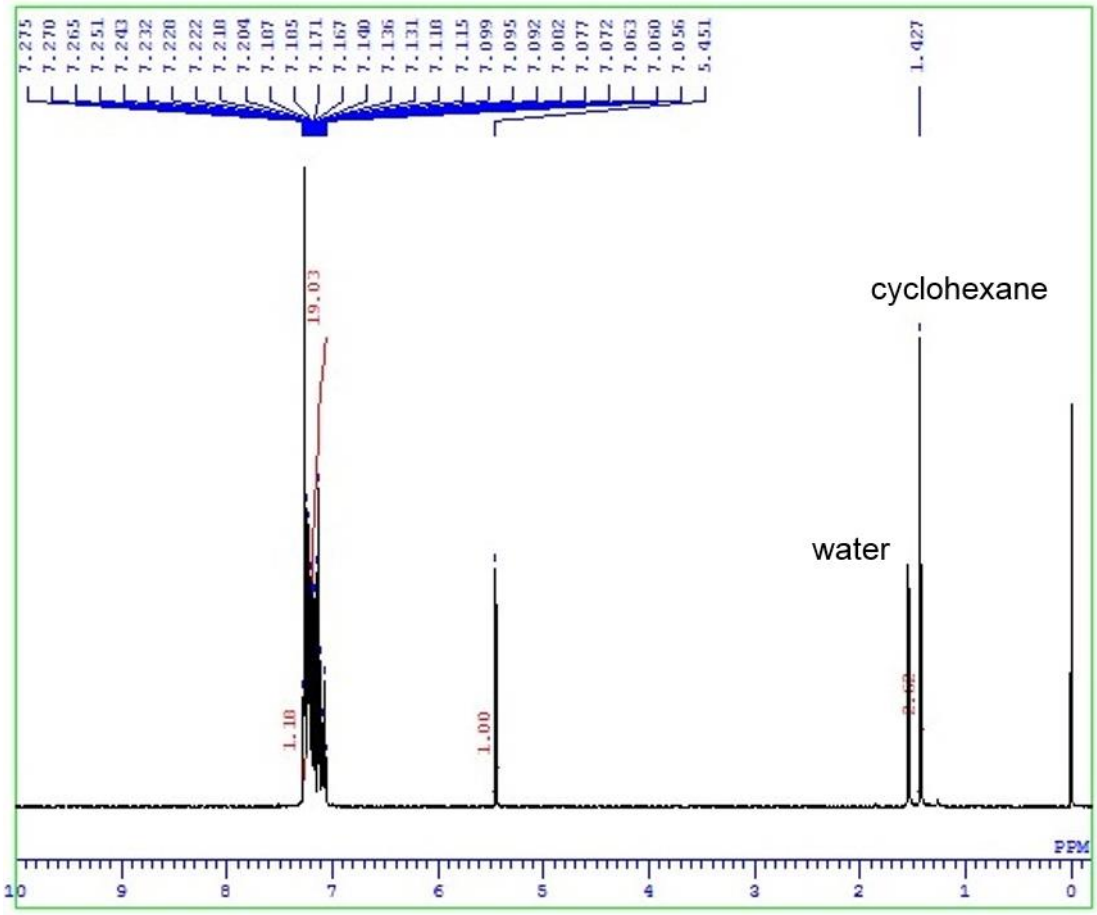

Figure S3. ^{1}H NMR spectrum of phase $\mathbf{G_I^{cyclohexane}}$.

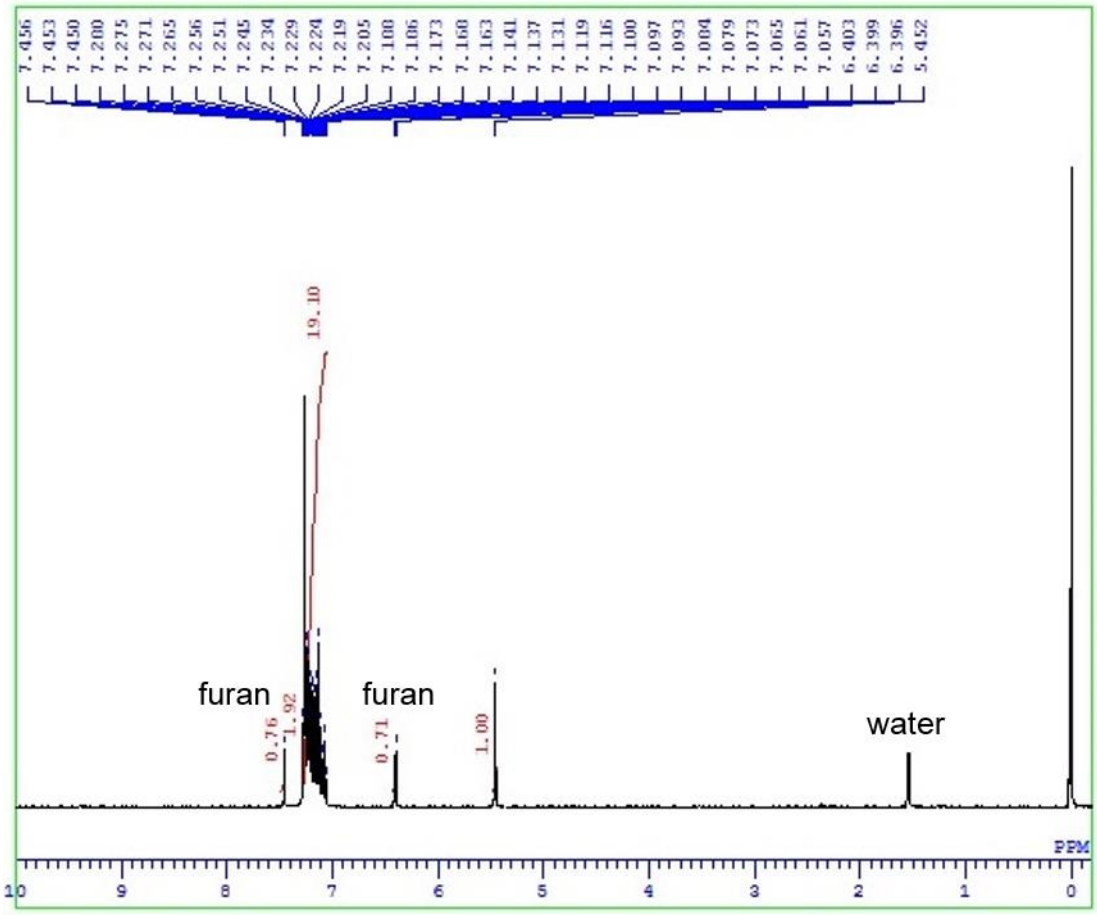

Figure S4. ^{1}H NMR spectrum of phase $\mathbf{G_I^{furan}}$.

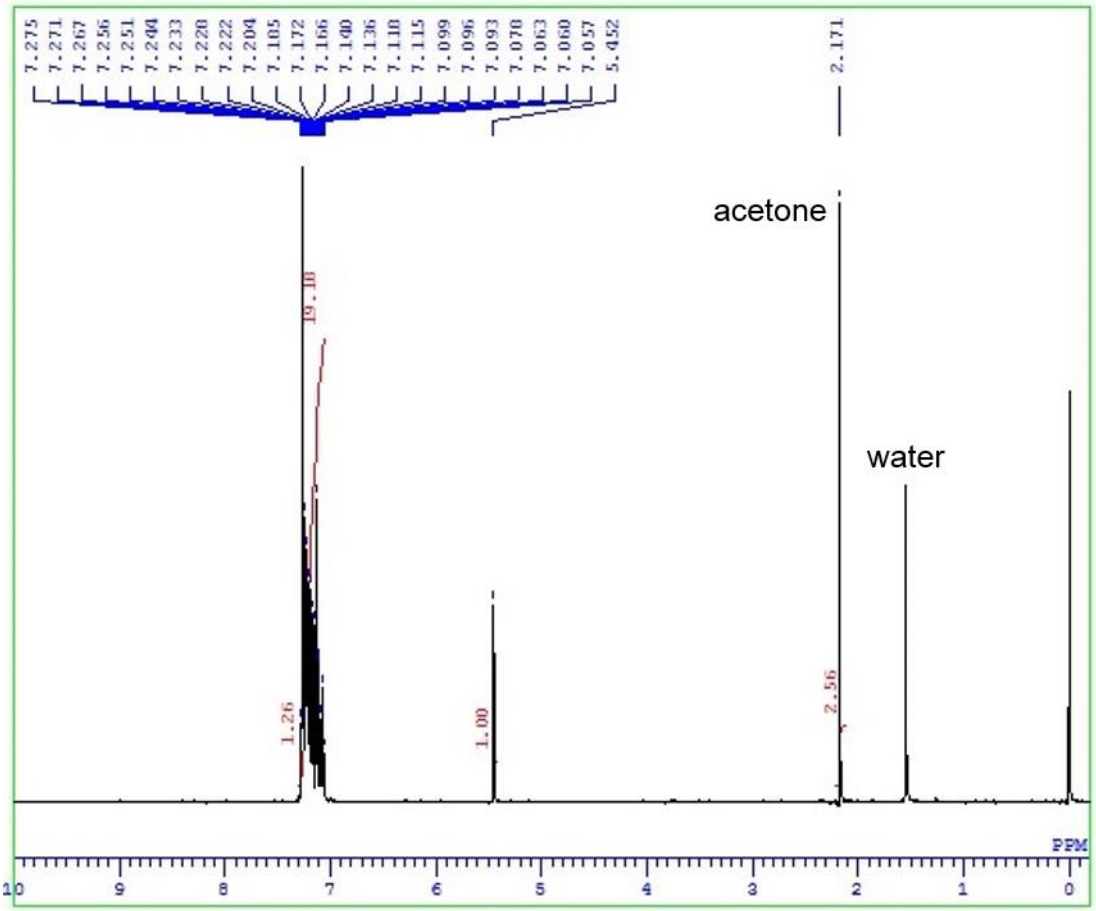

Figure S5. ^{1}H NMR spectrum of phase **GI^{acetone}**.

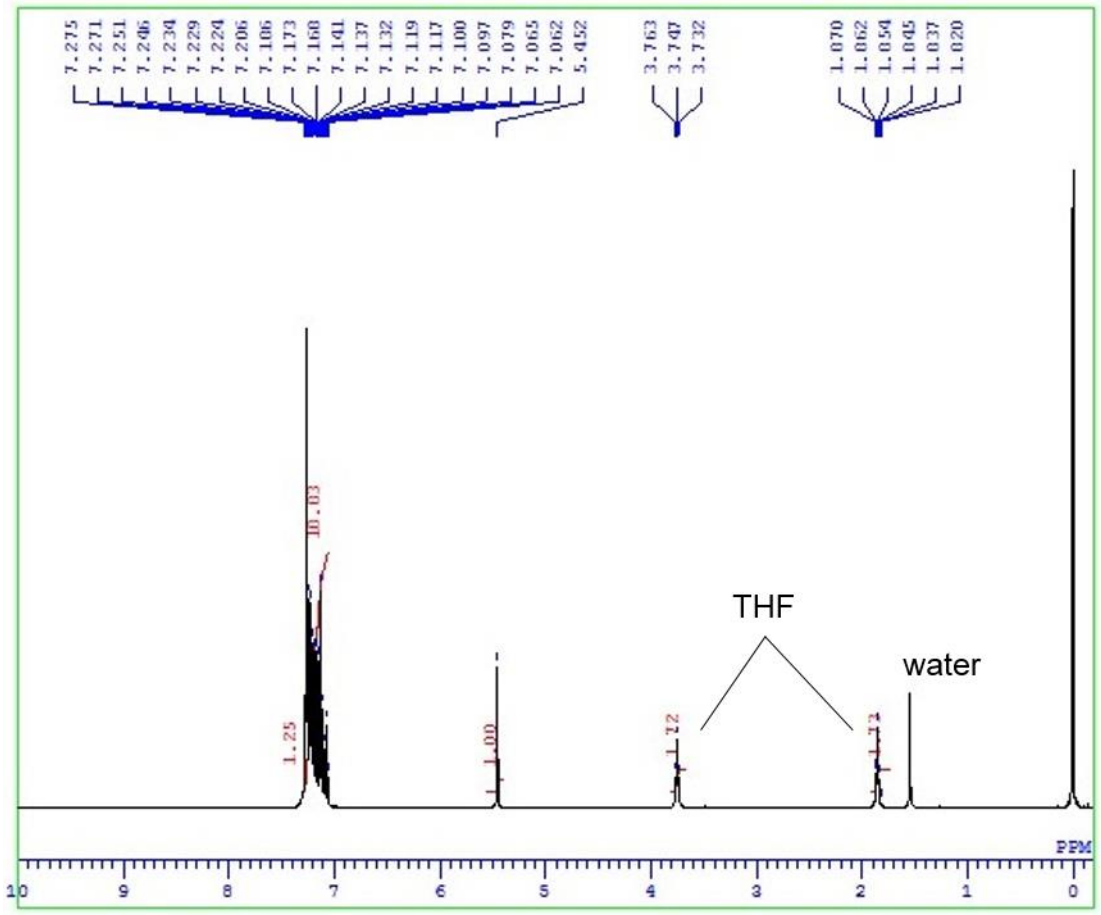

Figure S6. ^{1}H NMR spectrum of phase $\mathbf{G_I^{THF}}$.

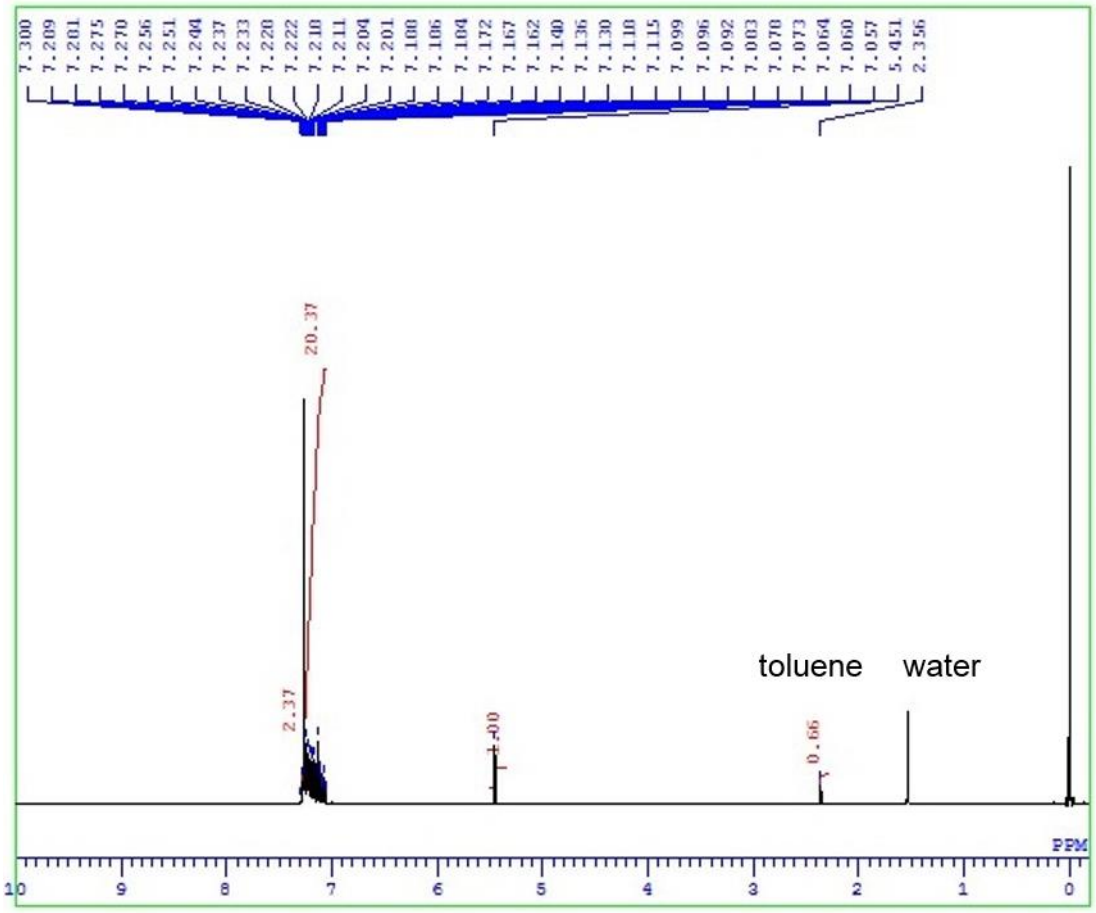

Figure S7. ^{1}H NMR spectrum of phase $\mathbf{G_{II}^{toluene}}$.

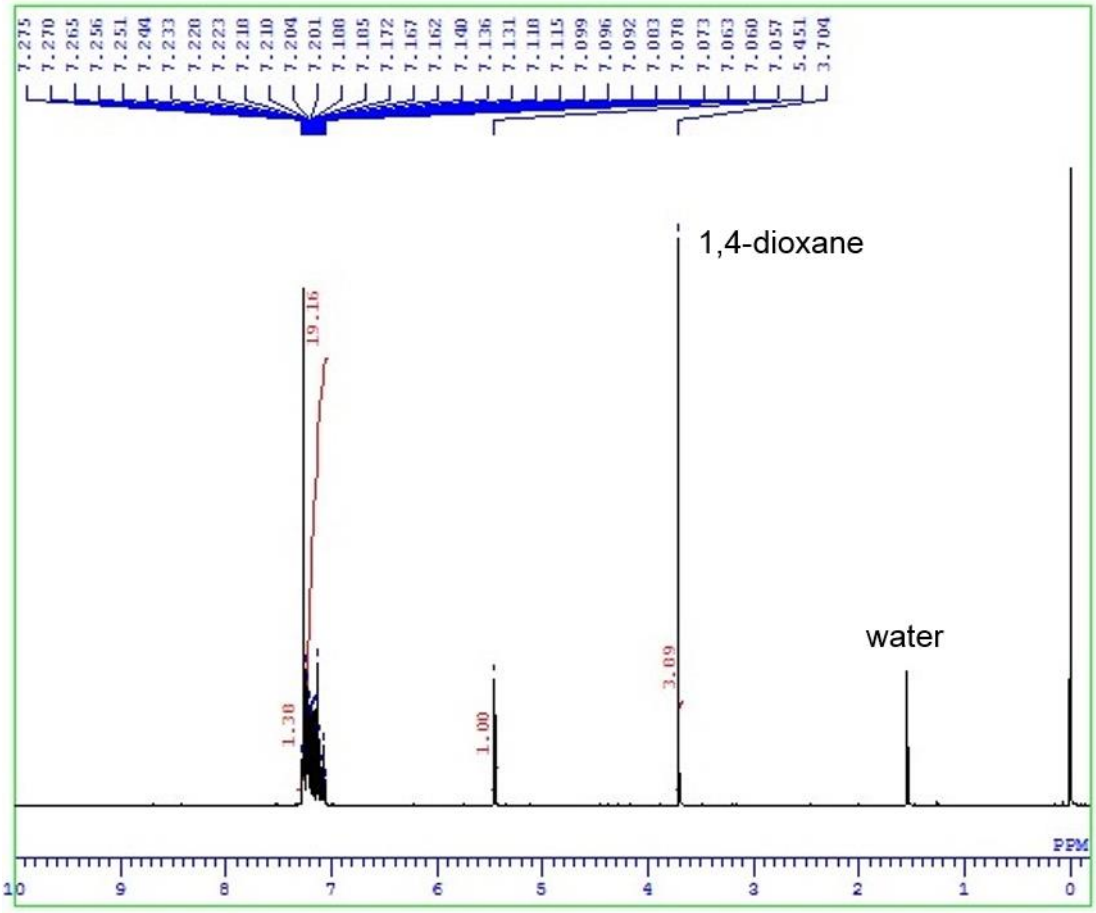

Figure S8. ^{1}H NMR spectrum of phase $\mathbf{G_{II}^{1,4\text{-dioxane}}}$.

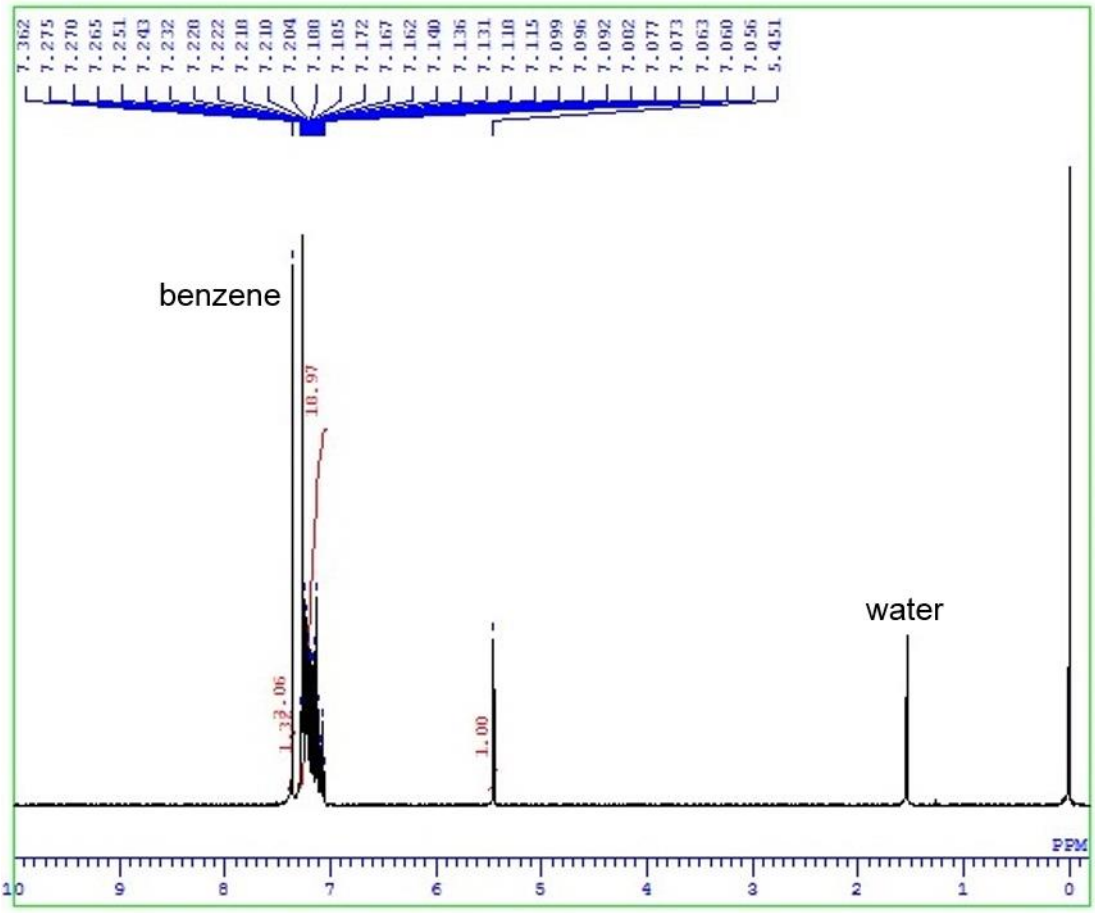

Figure S9. ^{1}H NMR spectrum of phase $\mathbf{G_{II}^{benzene}}$.

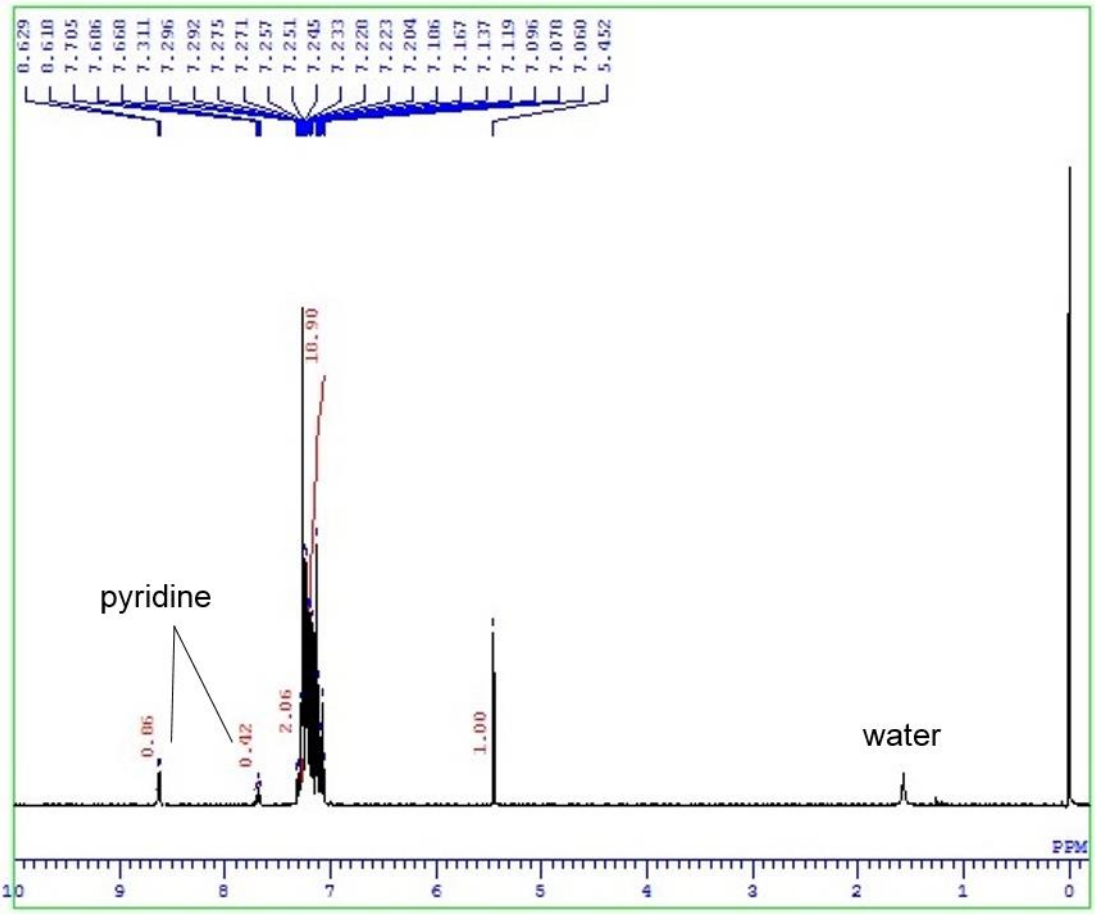

Figure S10. ^{1}H NMR spectrum of phase $\mathbf{G_{II}^{pyridine}}$.

Thermal Property Measurements

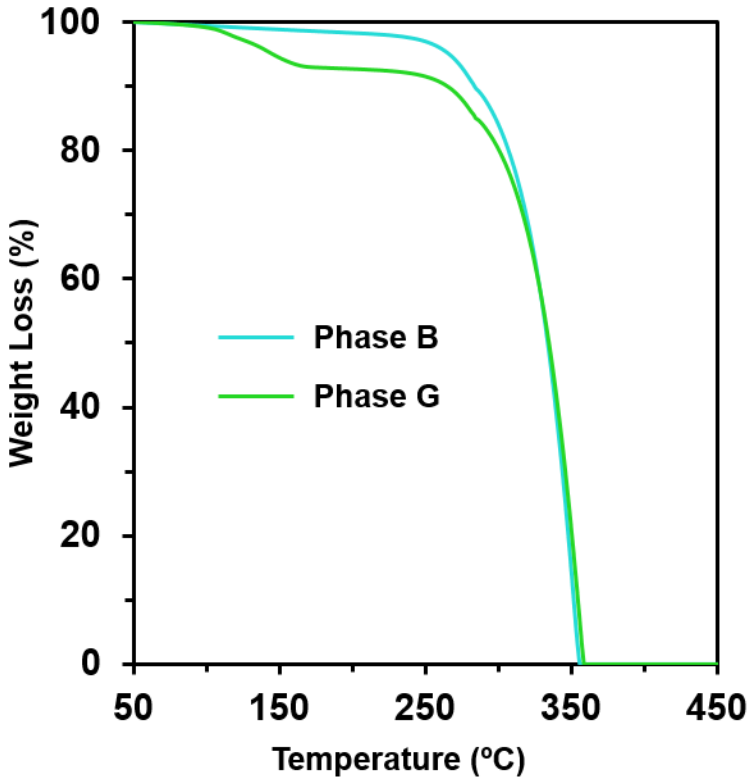

Figure S11. Tharmal gravimetric analysis (TGA) profiles of crystals **B** and **G**.

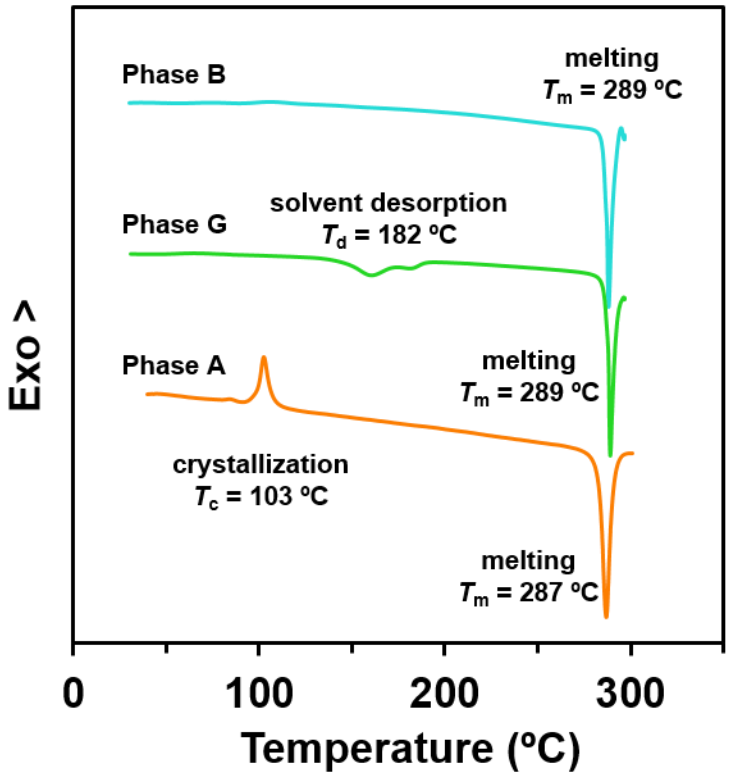

Figure S12. DSC curves of **2** in the crystalline phases **B** and **G** and the amorphous phase **A**.

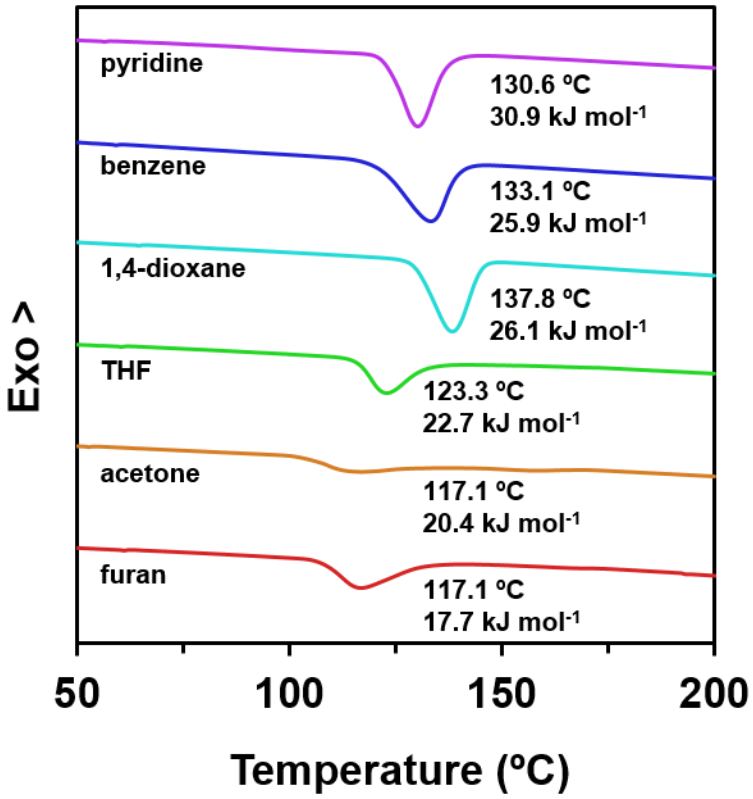

Figure S13. DSC curves of phases **G**$_{\mathbf{I}}$ (furan, acetone and THF) and **G**$_{\mathbf{II}}$ (1,4-dioxane, benzene and pyridine). Transition temperatures (T_{trans}) and enthalpy changes (ΔH_{trans}) are shown at the corresponding peak positions.

Optical Property Measurements

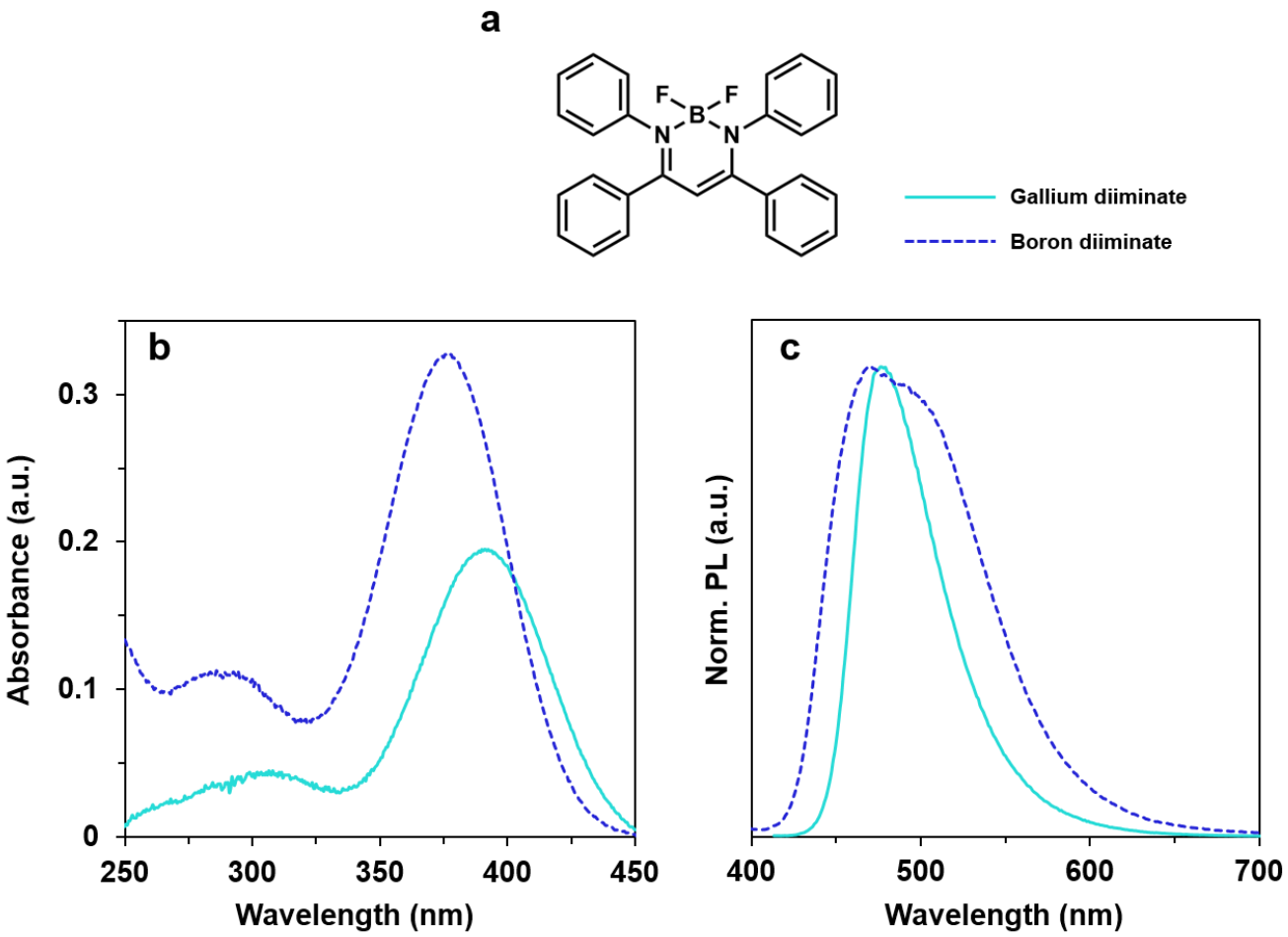

Figure S14. (a) Chemical structure of boron diiminate. (b) The absorption spectra in THF (1.0×10^{-5} M) and (c) the PL spectra in their crystalline states of boron and gallium diiminates with the excitation light at the corresponding absorption maxima in the solution state.

Table S1. Optical properties of gallium and boron diiminate complexes

	$\lambda_{abs.}$ (nm) [b]	$\varepsilon \times 10^4$ (M^{-1} cm^{-1}) [c]	λ_{PL} (nm) [a,d]	Φ_{PL} [b,f]	Φ_{PL} [d,e]	τ [d,f]
gallium complex	382	1.95	476	< 0.01	0.48	2.94 (99.27%) 0.23 (0.73%) (χ^2 = 1.06)
boron complex	376	3.27	473	< 0.01	0.23	1.9 (100%) (χ^2 = 1.06)

[a] Excited at $\lambda_{abs.}$. [b] Measured in THF (1×10^{-5} M). [c] Molar absorption coefficients of the absorption maxima at longer wavelength region. [d] Measured in the crystalline state. [e] Determined using the integrated sphere method. [f] Excited at 375 nm by using UV diode laser and monitored at λ_{PL}.

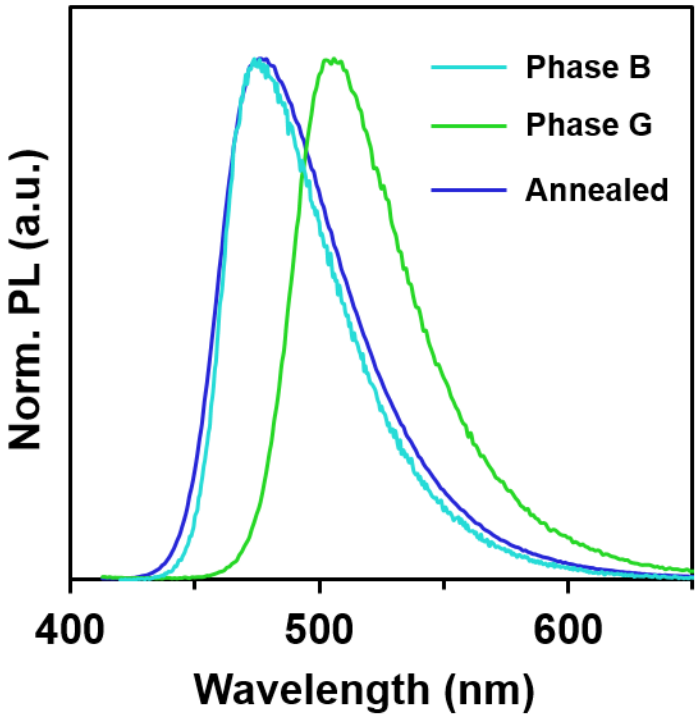

Figure S15. Photoluminescence spectra of crystals **B** and **G** and the annealed sample at 230 °C.

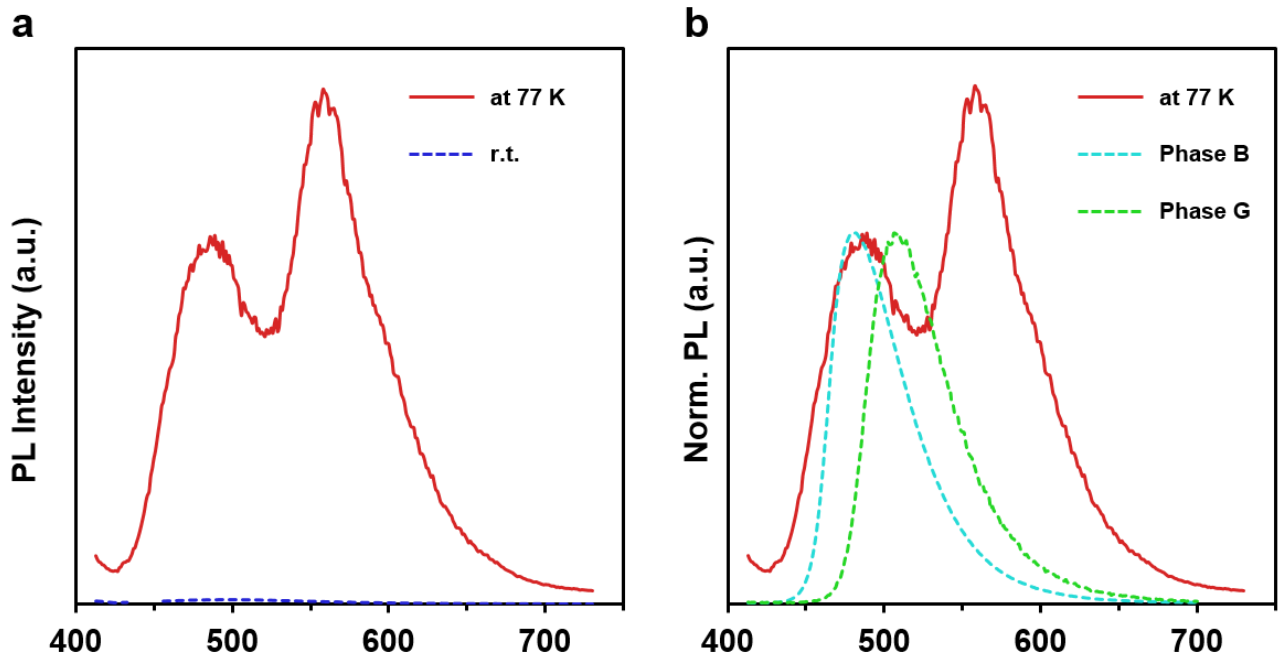

Figure S16. (a) PL spectra of **2** in 2Me-THF at 77K (red solid line) and at room temperature (blue dashed line). (b) Normalized PL spectra of **2** in 2Me-THF at 77 K and phases **B** and **G**.

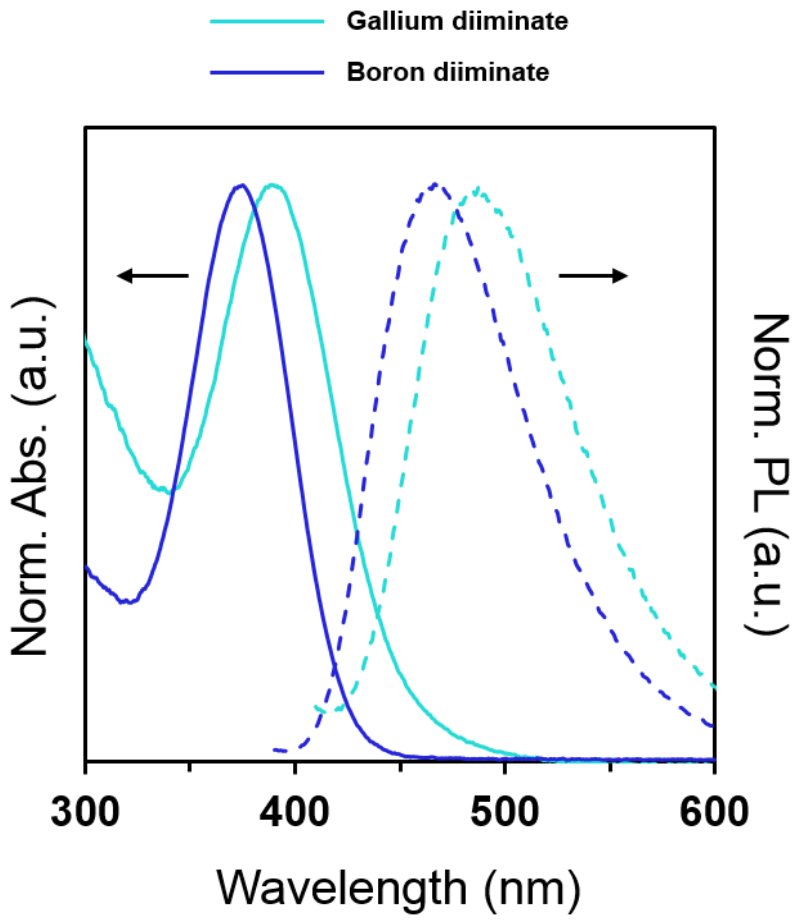

Figure S17. UV–vis (solid lines) and photoluminescence (dashed lines) spectra of the PMMA films containing 1 wt% gallium (cyan) and boron (blue) diiminate complexes.

Table S2. Optical properties of PMMA films containing gallium and boron complexes

	λ_{abs} (nm)	λ_{PL} (nm) [a]	Φ_{PL} [a,b]	τ (ns) [c]
gallium complex	390	485	0.12	0.96 (28%) 2.88 (72%)
boron complex	375	468	0.13	1.00 (24%) 2.91 (76%)

[a] Excited at corresponding $\lambda_{abs.}$ [b] Determined using integrated sphere method. [c] Excited at 375 nm by using UV diode laser and monitored at λ_{PL} of each sample.

Diffuse Reflectance Spectra

Transformation with the Kubelka-Munk equation

The diffuse reflectance spectra were transformed with the following Kubelka-Munk equation.[2]

$$f(r_\infty) = \frac{(1 - r_\infty)^2}{2r_\infty} = \frac{K}{S}$$

Here, r_∞ is a relative reflectance (= r_∞^{sample} / $r_\infty^{\text{standard}}$, r_∞^{sample} and $r_\infty^{\text{standard}}$ are reflectances of samples and the barium sulfate standard white plate), K is an absorption coefficient of samples, and S is a scattering coefficient of samples.

Deconvolution protocol for diffuse reflection spectrum of phase **B**:

The diffuse reflectance spectrum from phase **B** was deconvoluted by the least-squares method with following one-component Gaussian function, $f(\nu)$, in the region from 14,300 cm^{-1} to 27,500 cm^{-1}.

$$f(\nu) = A_1 \exp[-(\nu - \nu_0)^2 / w_1^2]$$

Here, ν is a wavenumber in the unit of cm^{-1}, A_1 is a magnitude, ν_0 is a wavenumber at the absorption maxima, and w_1 is a full width at the half maximum (FWHM). A_1 and w_1 were optimized as variables, whereas ν_0 was a constant.

Deconvolution protocol for the others:

The diffuse reflection spectra of the others were deconvoluted by the least-squares method with following two-component Gaussian function, $f(\nu)$, in the region from 14,300 cm^{-1} to 27,500 cm^{-1}.

$$f(\nu) = A_1 \exp[-(\nu - \nu_0)^2 / w_1^2] + A_2 \exp[-(\nu - \nu_2)^2 / w_2^2]$$

Here, ν is a wavenumber, A_1 and A_2 are magnitudes, ν_0 is a wavenumber at the absorption maxima of phase **B**, ν_2 is a wavenumber at the maxima of additional component, and w_1 and w_2 are FWHMs. A_1, A_2, w_1, w_2 and ν_2 were optimized as variables, whereas ν_0 was constant.

Phase **B**

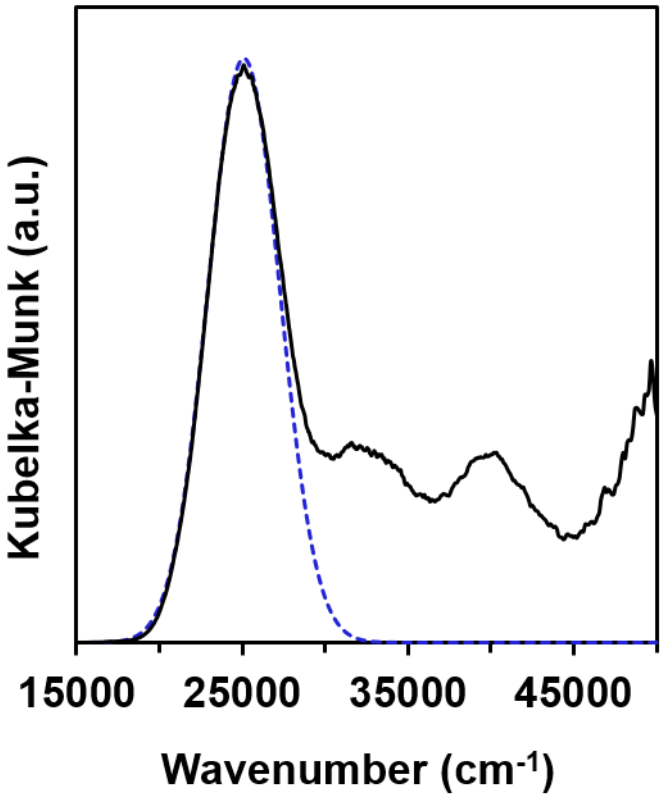

Figure S18. Diffuse reflection spectra observed from phase **B** (black solid line). The blue dashed line represents the deconvoluted Gaussian component.

Phase $\mathbf{G_I^{furan}}$

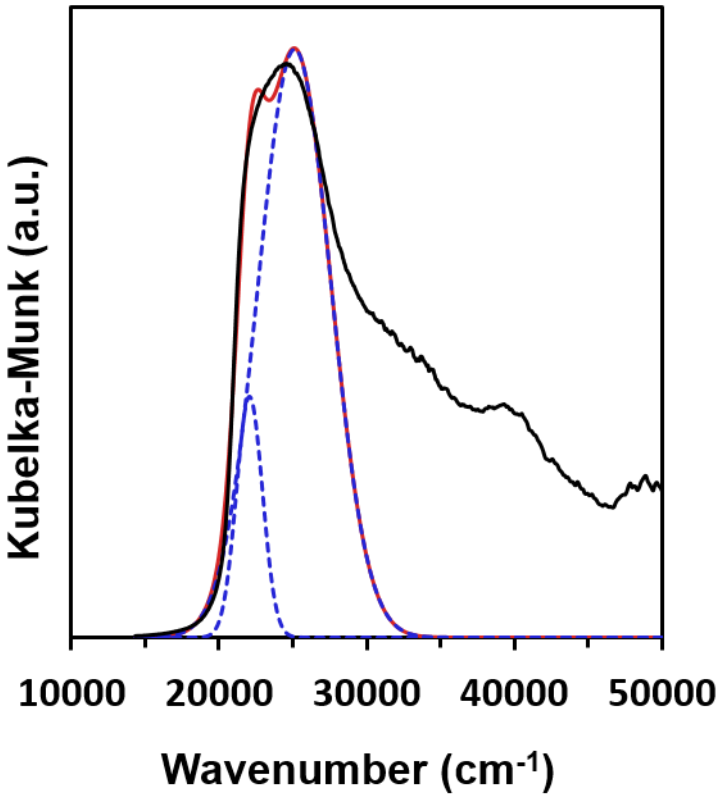

Figure S19. Diffuse reflection spectra observed from phase $\mathbf{G_I^{furan}}$ (black solid line). Blue dashed and red solid lines represent the deconvoluted Gaussian components and the sum of them, respectively.

Phase $\mathbf{G_I^{acetone}}$

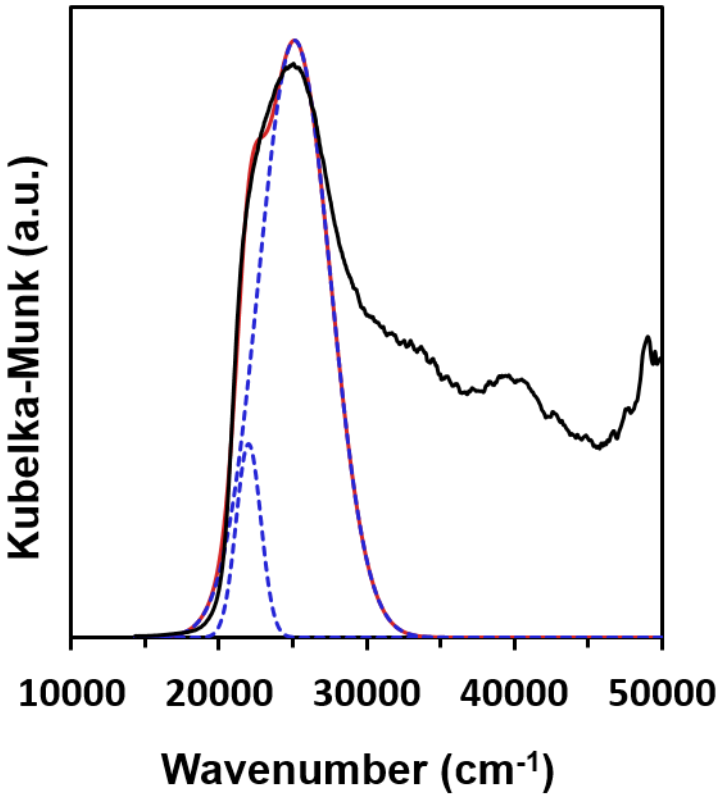

Figure S20. Diffuse reflection spectra observed from phase $\mathbf{G_I^{acetone}}$ (black solid line). Blue dashed and red solid lines represent the deconvoluted Gaussian components and the sum of them, respectively.

Phase $\mathbf{G_I^{THF}}$

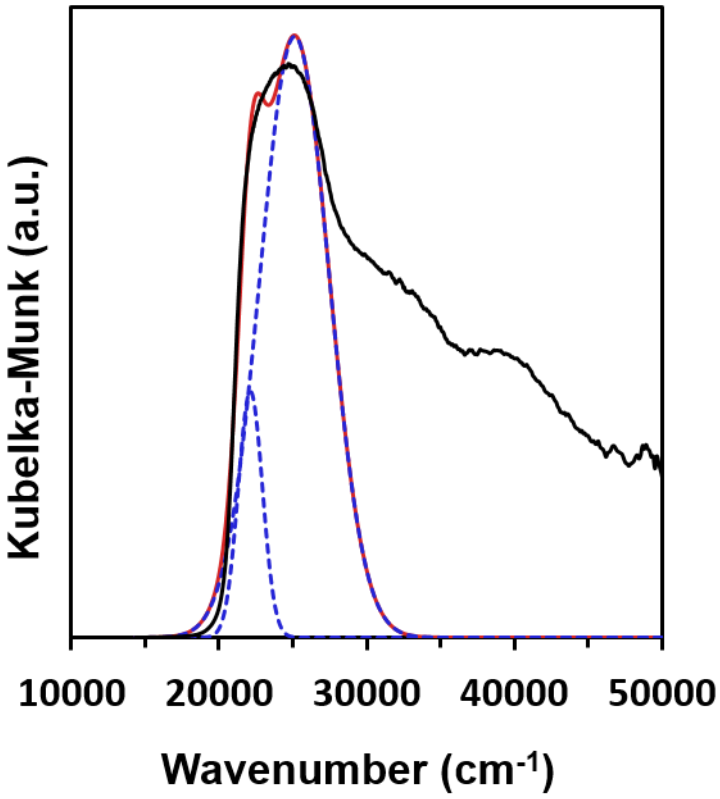

Figure S21. Diffuse reflection spectra observed from phase $\mathbf{G_I^{THF}}$ (black solid line). Blue dashed and red solid lines represent the deconvoluted Gaussian components and the sum of them, respectively.

Phase $\mathbf{G_{II}^{1,4\text{-dioxane}}}$

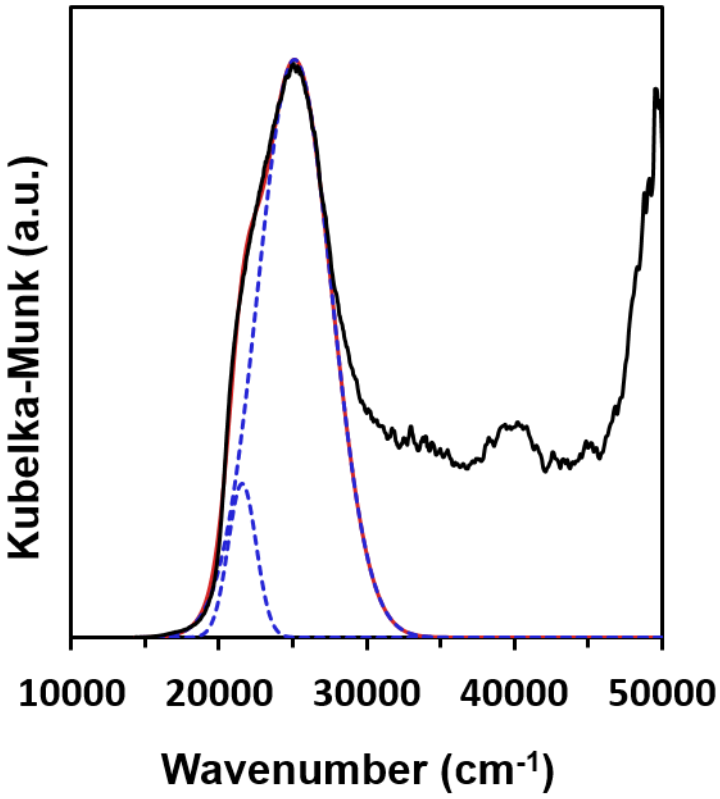

Figure S22. Diffuse reflection spectra observed from phase $\mathbf{G_{II}^{1,4\text{-dioxane}}}$ (black solid line). Blue dashed and red solid lines represent the deconvoluted Gaussian components and the sum of them, respectively.

Phase $\mathbf{G_{II}^{benzene}}$

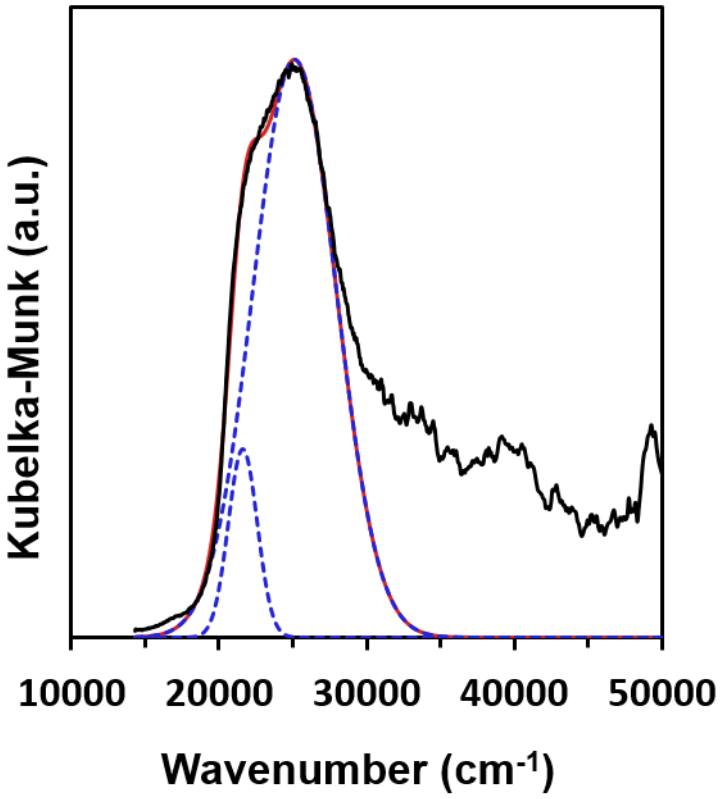

Figure S23. Diffuse reflection spectra observed from phase $\mathbf{G_{II}^{benzene}}$ (black solid line). Blue dashed and red solid lines represent the deconvoluted Gaussian components and the sum of them, respectively.

Phase $\mathbf{G_{II}^{pyridine}}$

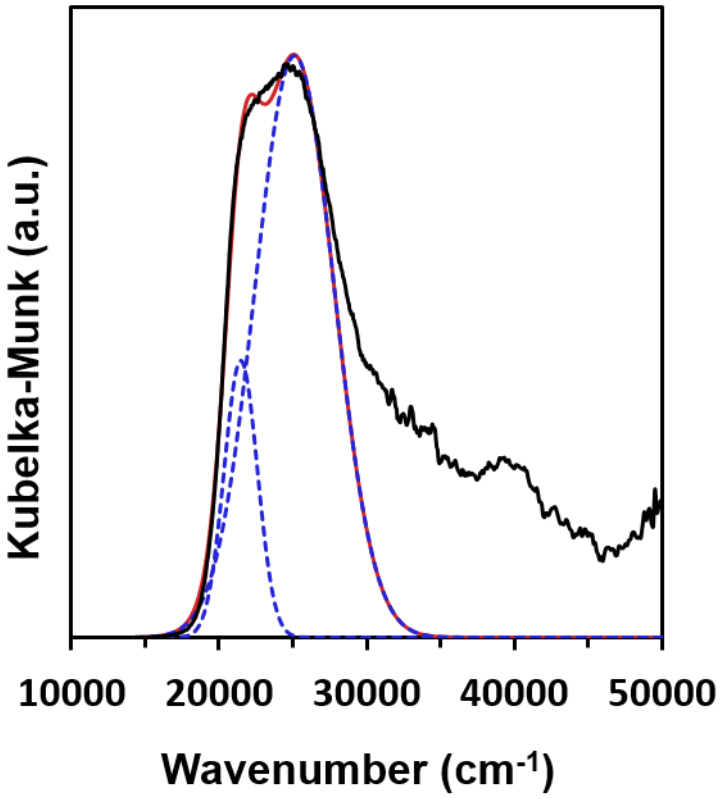

Figure S24. Diffuse reflection spectra observed from phase $\mathbf{G_{II}^{pyridine}}$ (black solid line). Blue dashed and red solid lines represent the deconvoluted Gaussian components and the sum of them, respectively.

Table S3. Results of deconvolution with the diffuse reflectance spectra

	A_1 (a.u.)	w_1 (cm^{-1})	A_2 (a.u.)	w_2 (cm^{-1})	v_2 (cm^{-1})	J [a]	$S_2 / (S_1 + S_2)$ [b]
Phase **B**	1.0096	3057.6	–	–	–	0.09675	–
$\mathbf{G_I^{furan}}$	1.0255	3464.1	0.42071	1251.9	22037	0.42342	0.1291
$\mathbf{G_I^{acetone}}$	1.0407	3420.4	0.33679	1185.9	21975	0.45789	0.1009
$\mathbf{G_I^{THF}}$	1.0484	3299.7	0.42873	1163.4	22098	0.73646	0.1260
$\mathbf{G_{II}^{1,4\text{-}dioxane}}$	1.0084	3511.0	0.26884	1341.6	21543	0.12007	0.09246
$\mathbf{G_{II}^{benzene}}$	1.0072	3970.6	0.32806	1389.4	21586	0.18741	0.1023
$\mathbf{G_{II}^{pyridine}}$	1.0145	3764.7	0.48153	1592.1	21450	0.17928	0.1672

[a] $J = \Sigma \mid \text{measured data} - f(v) \mid^2$. [b] S_1 and S_2 represent the areas of the first and second terms of deconvolution function, respectively.

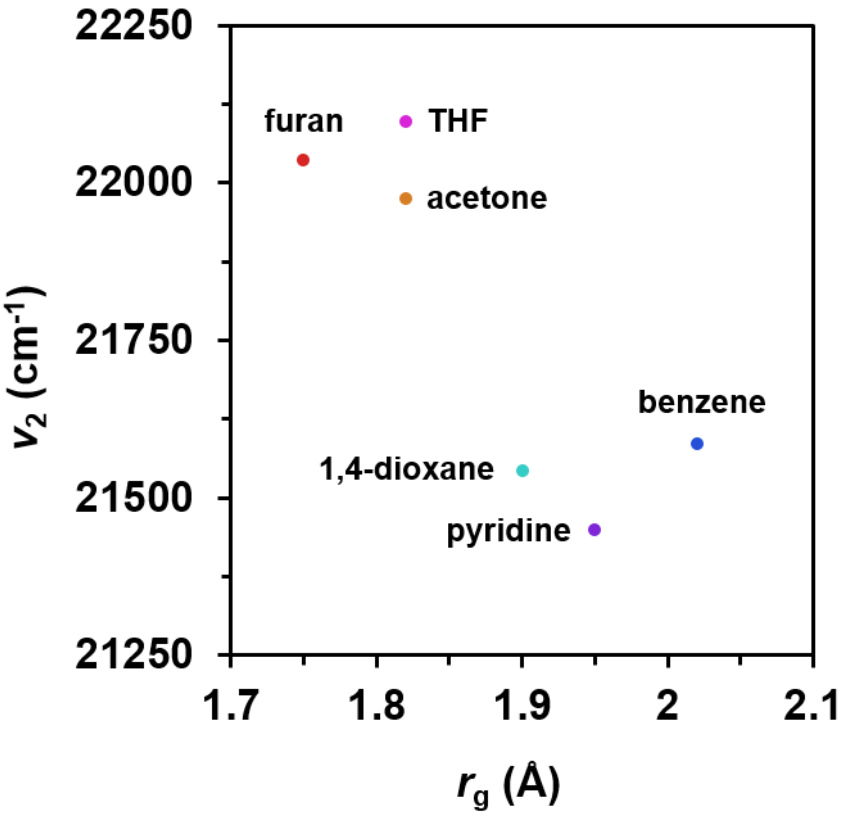

Figure S25. Relationships between radius of gyration (r_g) and new peak positions (ν_2).

The Properties of Solvents

Table S4. The numbers of captured VOCs after fuming with the phase **B** sample[a]

	C_6H_{12}	toluene	furan	$C_4H_8O_2$	acetone	benzene	THF	pyridine
ratio	0.25	0.3	0.5	0.5	0.5	0.5	0.5	0.5

[a] Calculated from the integral ratio in ^{1}H NMR spectra.

Table S5. Vapor pressures of VOCs[3]

	MeOH	DCM	MeCN	furan	acetone	THF	$C_4H_8O_2$	C_5H_5N	
p (kPa)	17	57	12	80	31	22	3.9	2.8	
	C_6H_6	C_6H_{12}	diacetyl	C_5H_{12}	C_6H_5Cl	$C_6H_5CH_3$	C_6H_5Br	C_6H_{14}	C_6H_5I
p (kPa)	13	13	7.6	68	1.6	3.8	0.56	20	0.14

Table S6. Dipole moments of VOCs

	MeOH	DCM	MeCN	furan	acetone	THF	$C_4H_8O_2$	C_5H_5N	
μ (D)	1.664	1.14	3.44	0.67	2.69	1.70	0	2.23	
	C_6H_6	C_6H_{12}	diacetyl	C_5H_{12}	C_6H_5Cl	$C_6H_5CH_3$	C_6H_5Br	C_6H_{14}	C_6H_5I
μ (D)	0	0	1.05	0	1.54	0.37	1.71	0.08	1.70

Table S7. Radius of gyrations of VOCs[a]

	MeOH	DCM	MeCN	furan	acetone	THF	$C_4H_8O_2$	C_5H_5N	
r_g (Å)	1.27	1.48	1.59	1.75	1.82	1.82	1.90	1.95	
	C_6H_6	C_6H_{12}	diacetyl	C_5H_{12}	C_6H_5Cl	$C_6H_5CH_3$	C_6H_5Br	C_6H_{14}	C_6H_5I
r_g (Å)	2.02	2.05	2.10	2.24	2.28	2.33	2.65	2.68	2.98

[a] Calculated from the optimized structures (B3LYP/6-31G level).

Table S8. Optical properties of the fumed samples

	Φ_{PL} [a,b]	$\lambda_{PL,max}$ (nm) [b]	τ (ns) [c]
cyclohexane	0.20	496	1.24 (15.37%) 2.79 (84.63%)
toluene	0.20	500	1.18 (30.52%) 2.60 (69.48%)
furan	0.14	501	0.829 (88.57%) 1.78 (11.43%)
1,4-dioxane	0.12	506	0.659 (27.20%) 1.45 (72.80%)
acetone	0.12	506	0.812 (69.36%) 1.35 (30.64%)
benzene	0.12	508	0.675 (0.51%) 1.01 (99.49%)
THF	0.09	509	0.807 (81.90%) 1.61 (18.10%)
pyridine	0.06	512	0.245 (8.50%) 0.618 (91.50%)

[a] Absolute quantum yield. [b] Measured in solid states with the excitation light at 393 nm. [c] Measured in the solid states with the excitation light at 375 nm and monitored at each emission maximum wavelength.

Dipole Moments

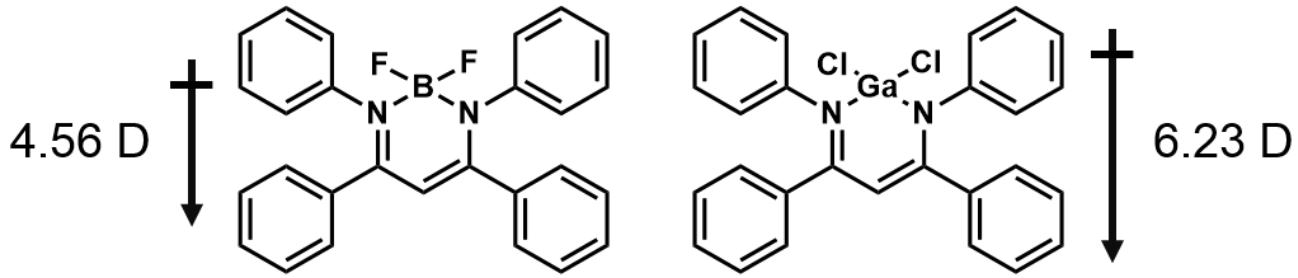

Figure S26. Dipole moments of diiminate complexes obtained by DFT calculations at 6-311G+(2d,p) level.

XRD Measurements

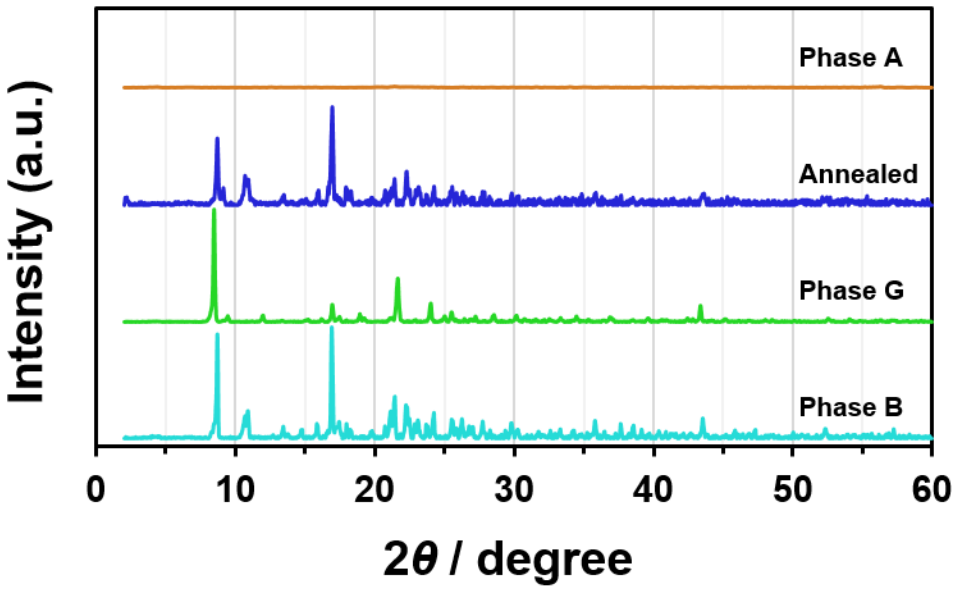

Figure S27. PXRD patterns of **2** in the crystallines **B** and **G** and amorphous **A**.

Rietveld Refinements

The analyzed PXRD data were measured using Rigaku SmartLab (CuKα_1 radiation λ = 1.54059 Å, transmittance mode), D/tex Ultra as a detector and capillary rotation attachment. The analyses were carried out with the powder X-ray diffraction analysis software, PDXL2. For all compounds, indexing programs, DICVOL[4] or ITO[5], were used for the determination of cell dimensions. The diffraction profiles were decomposed with the whole powder pattern fitting (WPPF) method. Following these data, corresponding space groups were determined on the basis of systematic extinctions. After additional WPPF methods, the initial states of phase **B** and **G** were obtained by direct space method with optimized structures of gallium diiminate (B3LYP/6-311G+(2d,p)) and THF (B3LYP/6-31G) molecules. For other phases, the initial structures were determined by the direct space method with the refined structure of phase **G** and the optimized structures of corresponding solvent molecules. These obtained structures were refined using the Rietveld method under restrained conditions for bond lengths and angles obtained from Cambridge Structural Database System (CSDS) via Mogul Server Ver. 1.0. Restraint stiffness, s_{res} (defined by Eq. 4), was determined as σ_{Norm} (defined by Eq. 8) becomes proximate value to one. We determined converged structure, confirming residual sum of squares, R_{wp}, was less than 10%, and goodness-of-fit indicator, S, sufficiently closed to one.

$$R_{\mathrm{p}} = \frac{\sum_i \left| y_i - y_i^{\mathrm{cal}}(\boldsymbol{p}) \right|}{\sum_i |y_i|} \qquad \ldots \text{Eq. 1}$$

$$R_{\mathrm{wp}} = \sqrt{\frac{\sum_i w_i \left(y_i - y_i^{\mathrm{cal}}(\boldsymbol{p}) \right)^2}{\sum_i w_i \, y_i^2}} \qquad \ldots \text{Eq. 2}$$

$$R_{\mathrm{e}} = \sqrt{\frac{N - p}{\sum_i w_i \, y_i^2}} \qquad \ldots \text{Eq. 3}$$

$$S = \frac{R_{\mathrm{wp}}}{R_{\mathrm{e}}} \qquad \ldots \text{Eq. 4}$$

$$R = R_{\mathrm{wp}} + s_{\mathrm{res}}(R_{\mathrm{res}}^{d} + R_{\mathrm{res}}^{a}) \qquad \ldots\text{Eq. 5}$$

$$R_{\mathrm{res}}^{d} = \sum_{i}^{M_d} \left(\frac{d_{0i} - d_i}{\sigma_i^{d}} \right)^2 \qquad \ldots\text{Eq. 6}$$

$$R_{\mathrm{res}}^{a} = \sum_{j}^{N_a} \left(\frac{a_{0i} - a_i}{\sigma_i^{a}} \right)^2 \qquad \ldots\text{Eq. 7}$$

$$\sigma_{\mathrm{Norm}} = \sqrt{\frac{R_{\mathrm{res}}^{d} + R_{\mathrm{res}}^{a}}{M + N}} \qquad \ldots\text{Eq. 8}$$

Here, y_i is a diffraction intensity, $y_i^{\mathrm{cal}}(\boldsymbol{p})$ is a calculated intensity, $\boldsymbol{p}$ is a parameter for the least-squares method, w_i is a weight, N is the number of data points, M_d is the number of restraints for bond length, and N_a is the number of restraints for bond angle. In addition, $d_{0\mathrm{i}}$ and $a_{0\mathrm{j}}$ are mean bond lengths and angles of similar structures, respectively. $\sigma_{\mathrm{i}}^{\mathrm{d}}$ and $\sigma_{\mathrm{j}}^{\mathrm{a}}$ are standard deviations of mean bond lengths and angles, respectively.

Phase **B**

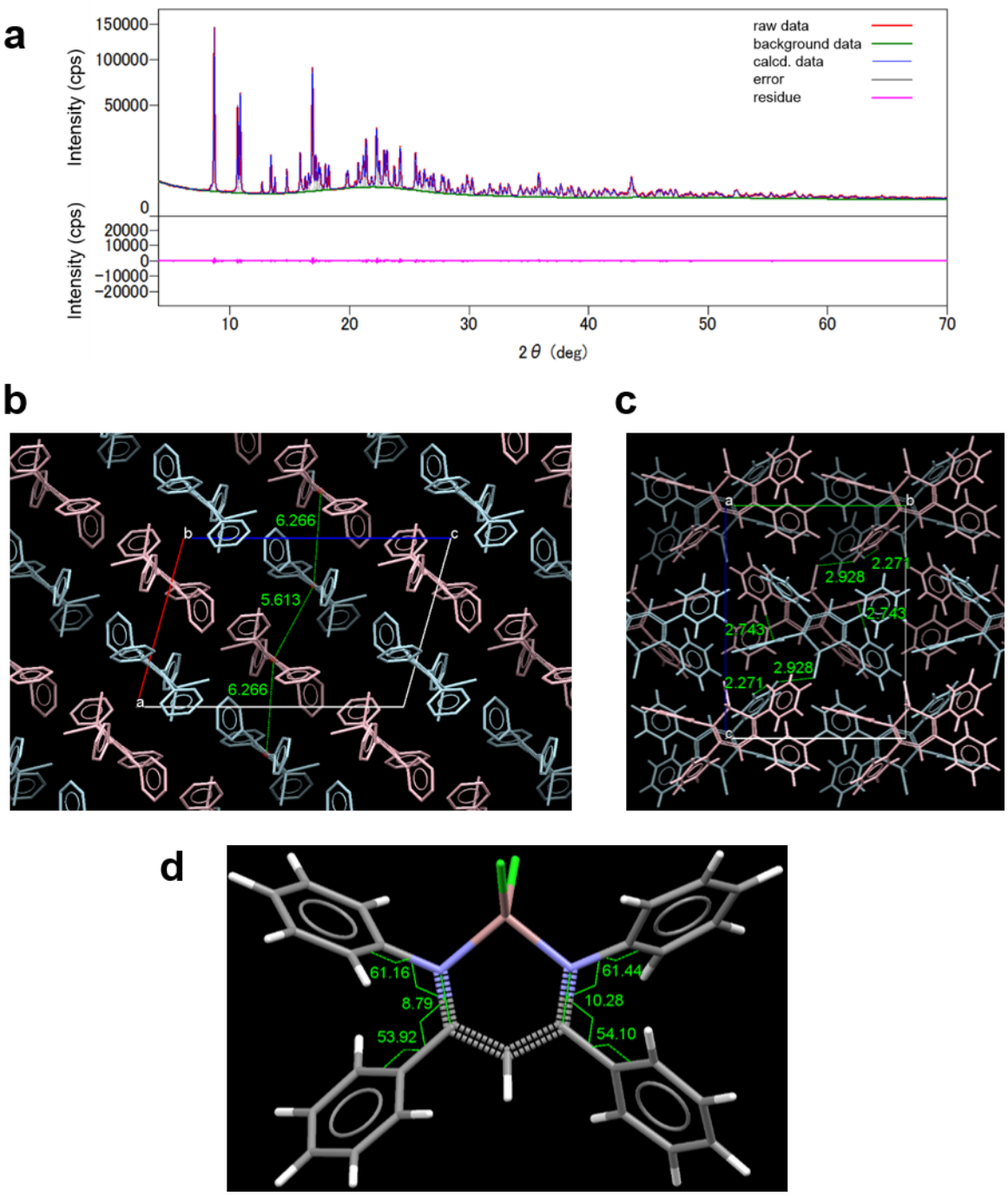

Figure S28. (a) Results of the Rietveld refinement of phase **B**. (b) Crystal structure along *b*-axis. Green labels indicate the distances (Å) between central six-membered rings of neighbors. Hydrogen atoms are omitted for clarity. (c) Crystal structure along *a*-axis. Green labels indicate the distances (Å) between contacting atoms; 2.271 Å: CH···HC, 2.743 Å: CH···π and 2.928 Å: CH···Cl. (d) Selected dihedral angles.

Table S9. Crystallographic data of phase **B**

parameters	Phase **B**
formula	C27 Cl2 Ga1 H21 N2
formula weight	514.098
crystal system	monoclinic
space group	$P2_1/n1$ (14)
a (Å)	11.29001(13)
b (Å)	12.86799(17)
c (Å)	17.2448(2)
α (deg)	90
β (deg)	105.6881(5)
γ (deg)	90
V (Å^3)	2411.99(5)
temperature (K)	298
Z	4
ρ_{calc} (g cm^{-3})	1.42
2θ range (deg)	4.000 – 46.500
R_{wp} (%)	3.17
R_p (%)	2.43
R_e (%)	2.20
S	1.4272

Phase **G** (identical to $\mathbf{G_I}^{THF}$)

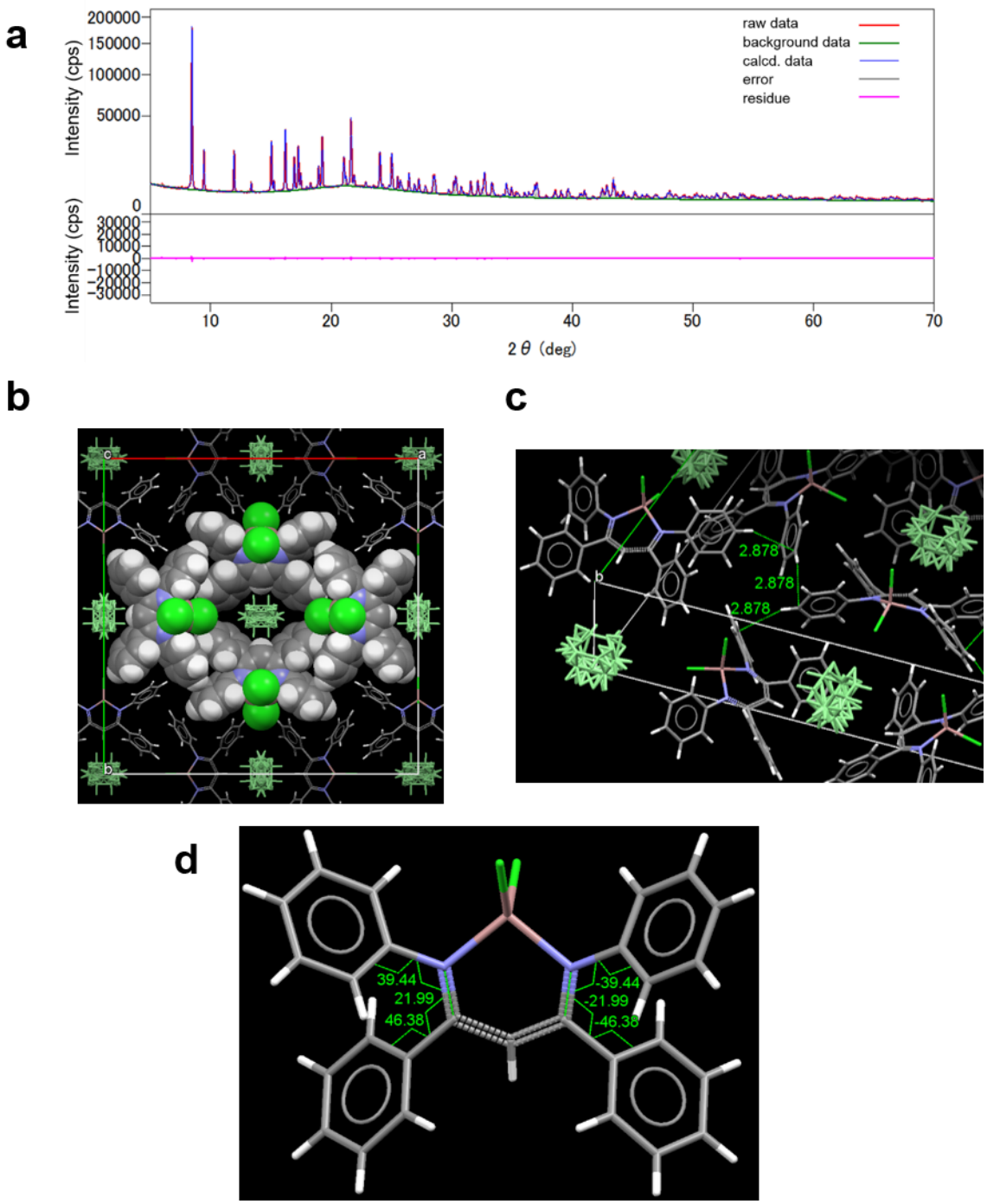

Figure S29. (a) Results of the Rietveld refinement of phase **G**. (b) Crystal structure along *c*-axis. Green molecules indicate adsorbed and disordered THF molecules. (c) Green labels indicate the distances (Å) between contacting atoms; 2.878 Å: CH···π. (d) Selected dihedral angles.

Table S10. Crystallographic data of phase **G** (**G**$_{\mathbf{I}}^{\mathrm{THF}}$)

parameters	Phase **G** and **G**$_{\mathbf{I}}^{\mathrm{THF}}$
formula	$C_{27}\ H_{21}Cl_2GaN_2\bullet(C_4H_8O)_{0.5}$
formula weight	550.151
crystal system	tetragonal
space group	$I4_1md$ (109)
a (Å)	29.6117(3)
b (Å)	29.6117(3)
c (Å)	6.01011(10)
α (deg)	90
β (deg)	90
γ (deg)	90
V (Å^3)	5270.00(12)
temperature (K)	298
Z	8
ρ_{calc} (g cm^{-3})	1.39
2θ range (deg)	5.000 – 40.000
R_{wp} (%)	2.81
R_p (%)	2.13
R_e (%)	2.34
S	1.1934

Phase $\mathbf{G_I}^{furan}$

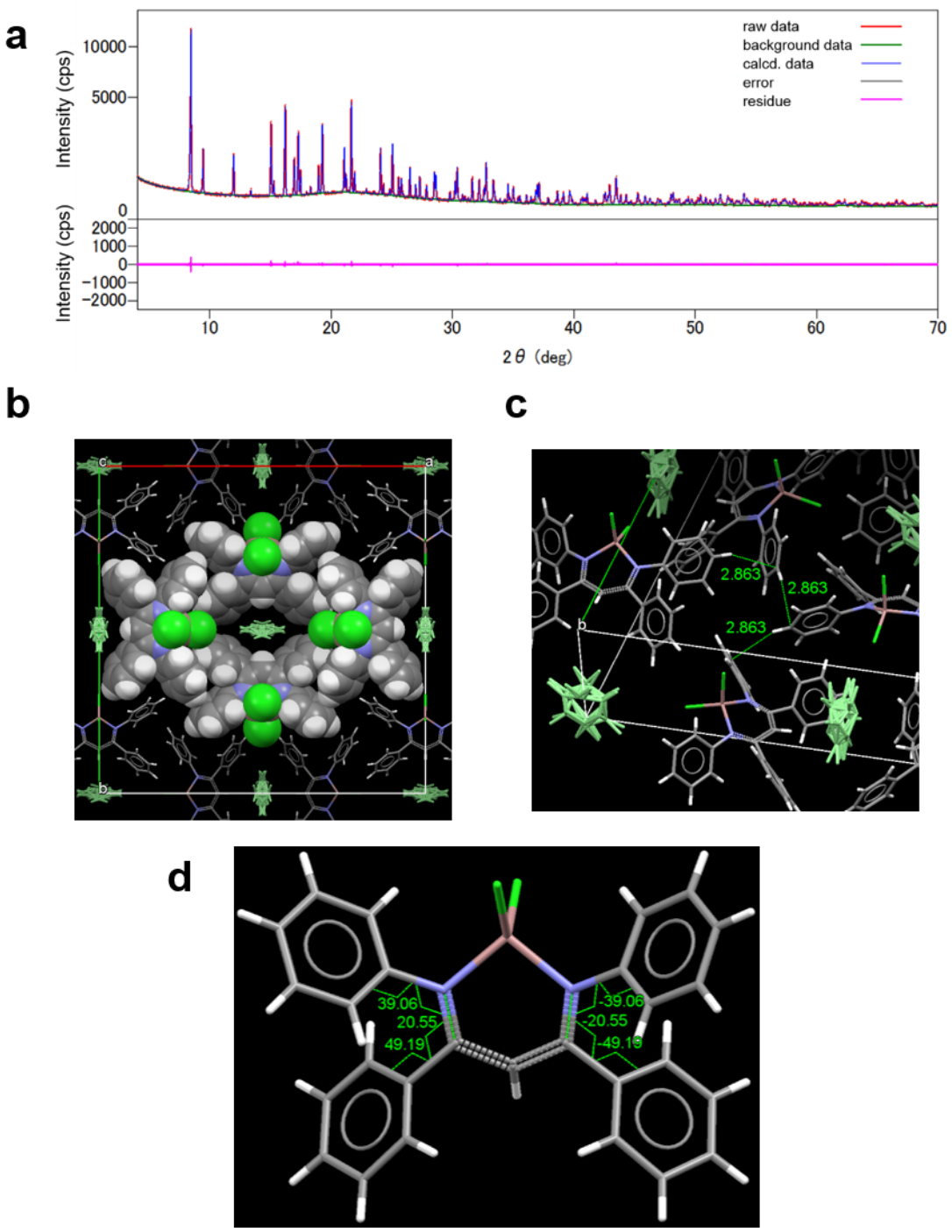

Figure S30. (a) Results of the Rietveld refinement of phase $\mathbf{G_I}^{furan}$. (b) Crystal structure along *c*-axis. Green molecules indicate adsorbed and disordered furan molecules. (c) Green labels indicate the distances (Å) between contacting atoms; 2.863 Å: CH···π. (d) Selected dihedral angles.

Table S11. Crystallographic data of phase $\mathbf{G_I}^{furan}$

parameters	Phase $\mathbf{G_I}^{furan}$
formula	$C_{27}\ H_{21}Cl_2GaN_2 \bullet (C_4H_4O)_{0.5}$
formula weight	545.132
crystal system	tetragonal
space group	$I4_1md$ (109)
a (Å)	29.5356(7)
b (Å)	29.5356(7)
c (Å)	5.99455(14)
α (deg)	90
β (deg)	90
γ (deg)	90
V (Å^3)	5229.3(2)
temperature (K)	298
Z	8
ρ_{calc} (g cm^{-3})	1.38
2θ range (deg)	4.000 – 42.500
R_{wp} (%)	5.36
R_p (%)	4.04
R_e (%)	5.12
S	1.0835

Phase **G**I^acetone

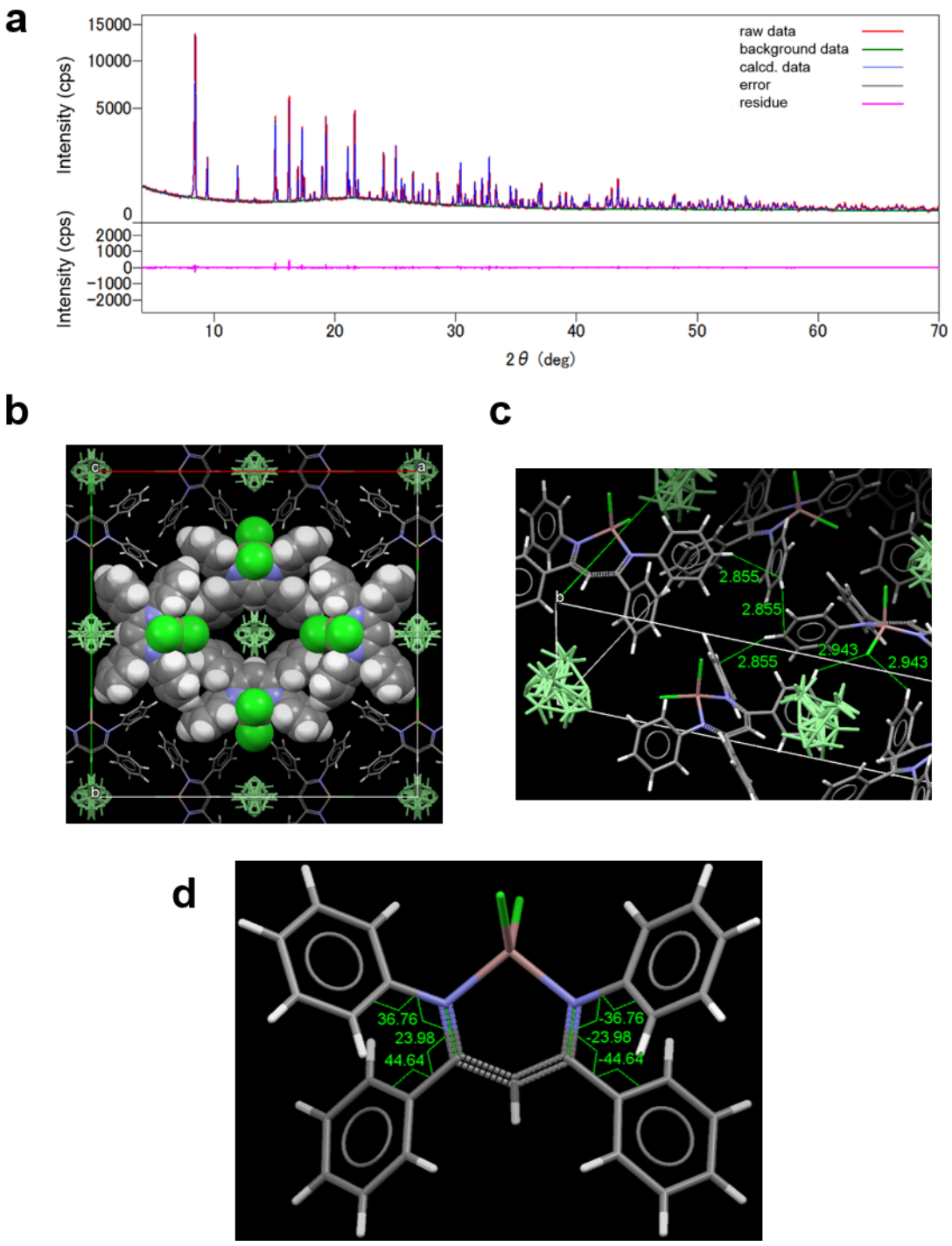

Figure S31. (a) Results of the Rietveld refinement of phase **G**I^acetone. (b) Crystal structure along *c*-axis. Green molecules indicate adsorbed and disordered acetone molecules. (c) Green labels indicate the distances (Å) between contacting atoms; 2.855 Å: CH···π and 2.943 Å: CH···Cl. (d) Selected dihedral angles.

Table S12. Crystallographic data of phase $\mathbf{G_I}^{acetone}$

parameters	Phase $\mathbf{G_I}^{acetone}$
formula	$C_{27}\ H_{21}Cl_2GaN_2 \bullet (C_3H_6O)_{0.5}$
formula weight	543.138
crystal system	tetragonal
space group	$I4_1md$ (109)
a (Å)	29.5810(2)
b (Å)	29.5810(2)
c (Å)	5.99452(5)
α (deg)	90
β (deg)	90
γ (deg)	90
V (Å^3)	5245.42(7)
temperature (K)	298
Z	8
ρ_{calc} (g cm^{-3})	1.38
2θ range (deg)	4.000 – 42.500
R_{wp} (%)	5.60
R_p (%)	4.17
R_e (%)	5.12
S	1.0864

Phase **G**$_{\mathbf{II}}^{1,4\text{-dioxane}}$

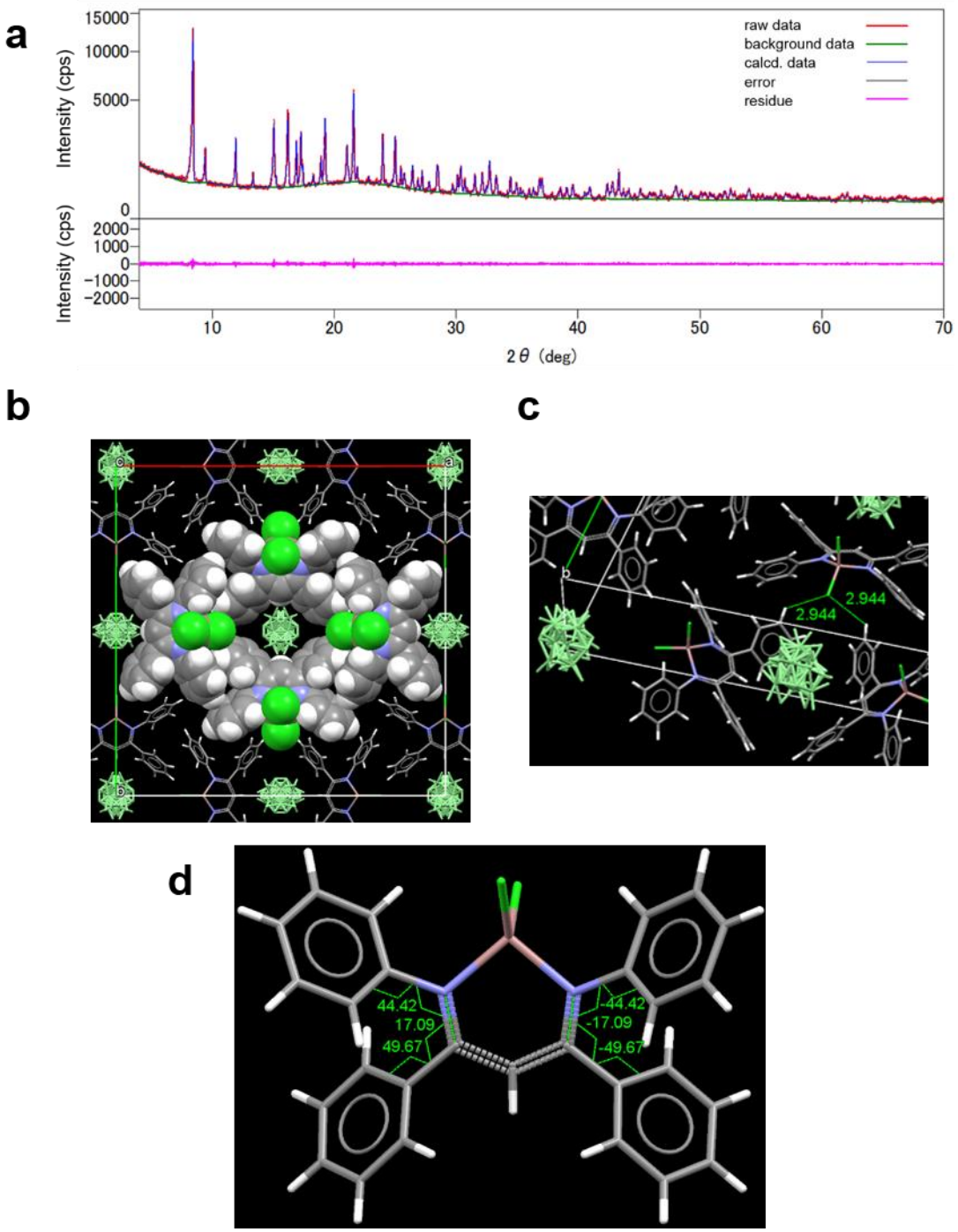

Figure S32. (a) Results of the Rietveld refinement of phase **G**$_{\mathbf{II}}^{1,4\text{-dioxane}}$. (b) Crystal structure along *c*-axis. Green molecules indicate adsorbed and disordered 1,4-dioxane molecules. (c) Green labels indicate the distances (Å) between contacting atoms; 2.944 Å: CH···Cl. (d) Selected dihedral angles.

Table S13. Crystallographic data of phase $\mathbf{G_{II}}'^{\text{4-dioxane}}$

parameters	Phase $\mathbf{G_{II}}'^{\text{4-dioxane}}$
formula	$C_{27}\ H_{21}Cl_2GaN_2 \bullet (C_4H_8O_2)_{0.5}$
formula weight	558.151
crystal system	tetragonal
space group	$I4_1md$ (109)
a (Å)	29.637(4)
b (Å)	29.637(4)
c (Å)	5.9954(9)
α (deg)	90
β (deg)	90
γ (deg)	90
V (Å^3)	5266.0(13)
temperature (K)	298
Z	8
ρ_{calc} (g cm^{-3})	1.41
2θ range (deg)	4.000 – 37.000
R_{wp} (%)	6.40
R_p (%)	4.85
R_e (%)	6.49
S	0.9616

Phase **G**II^{benzene}

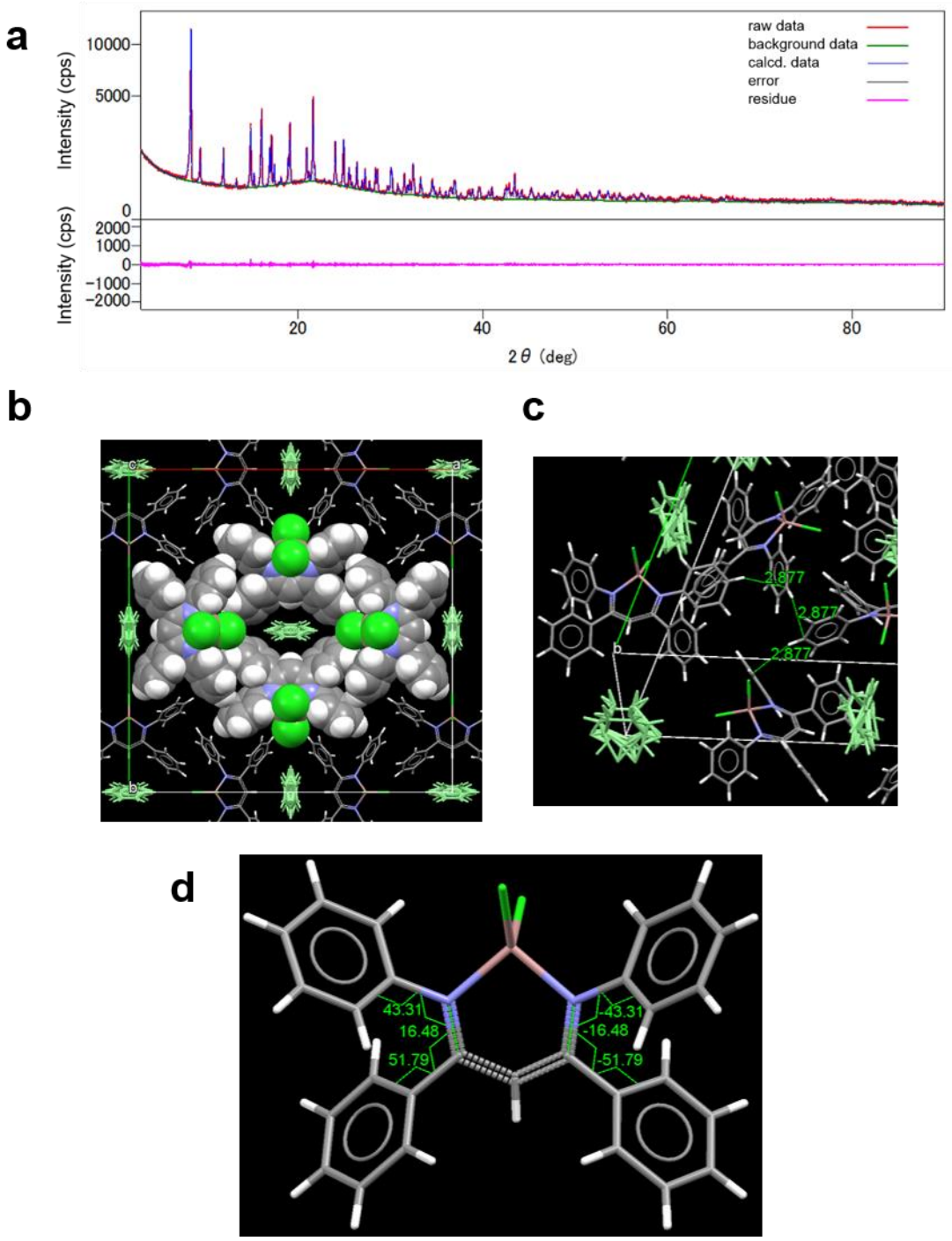

Figure S33. (a) Results of the Rietveld refinement of phase **G**II^{benzene}. (b) Crystal structure along *c*-axis. Green molecules indicate adsorbed and disordered benzene molecules. (c) Green labels indicate the distances (Å) between contacting atoms; 2.877 Å: CH···π. (d) Selected dihedral angles.

Table S14. Crystallographic data of phase $\mathbf{G_{II}}^{benzene}$

parameters	Phase $\mathbf{G_{II}}^{benzene}$
formula	$C_{27}\ H_{21}Cl_2GaN_2 \bullet (C_6H_6)_{0.5}$
formula weight	552.902
crystal system	tetragonal
space group	$I4_1md$ (109)
a (Å)	29.549(4)
b (Å)	29.549(4)
c (Å)	6.0559(8)
α (deg)	90
β (deg)	90
γ (deg)	90
V (Å^3)	5287.6(11)
temperature (K)	298
Z	8
ρ_{calc} (g cm^{-3})	1.39
2θ range (deg)	3.000 – 46.500
R_{wp} (%)	5.50
R_p (%)	4.10
R_e (%)	5.71
S	0.9592

Phase **G**II^{pyridine}

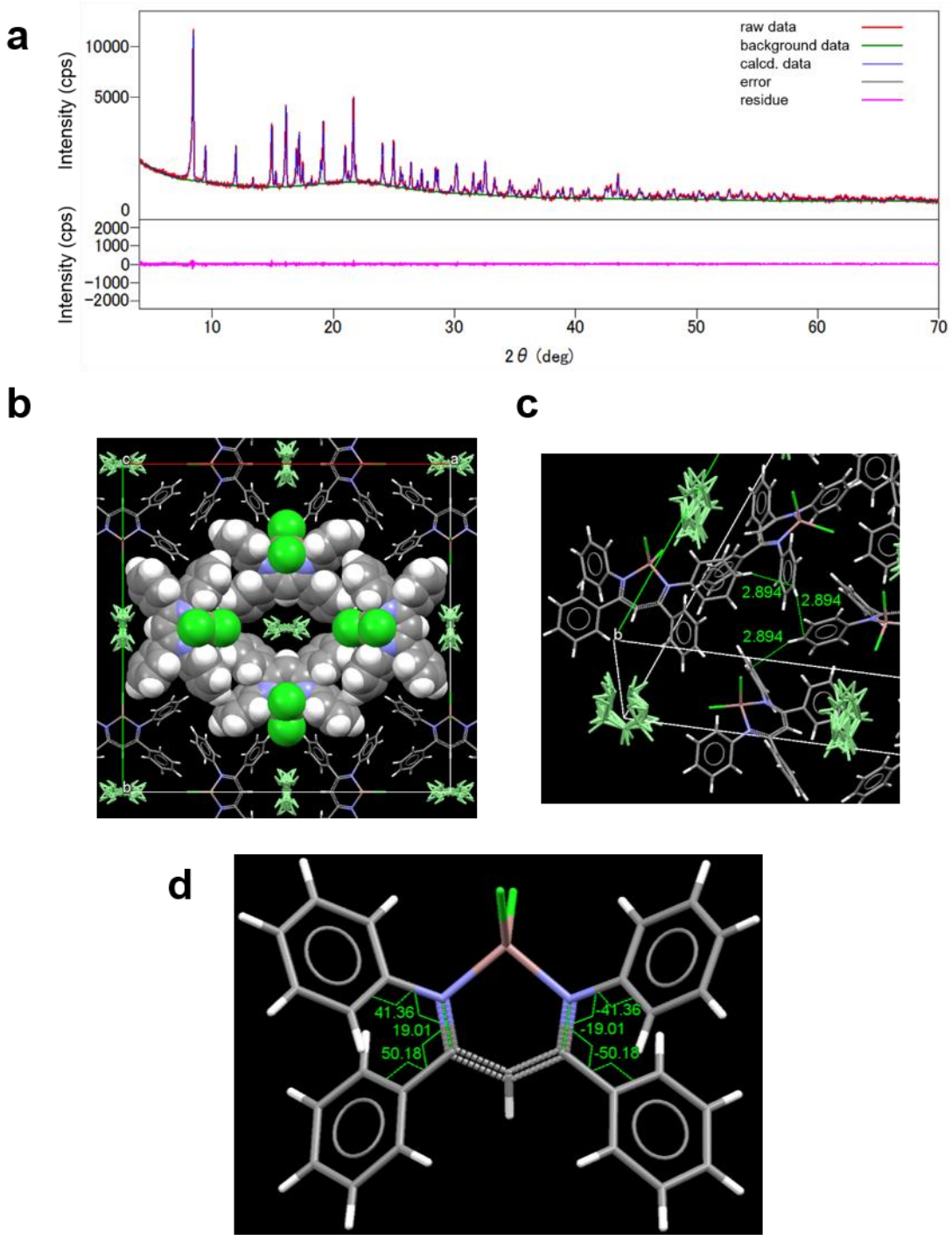

Figure S34. (a) Results of the Rietveld refinement of phase **G**II^{pyridine}. (b) Crystal structure along *c*-axis. Green molecules indicate adsorbed and disordered pyridine molecules. (c) Green labels indicate the distances (Å) between contacting atoms; 2.894 Å: CH···π. (d) Selected dihedral angles.

Table S15. Crystallographic data of phase $\mathbf{G_{II}}^{pyridine}$

parameters	Phase $\mathbf{G_{II}}^{pyridine}$
formula	$C_{27}\ H_{21}Cl_2GaN_2 \bullet (C_5H_5N)_{0.5}$
formula weight	553.648
crystal system	tetragonal
space group	$I4_1md$ (109)
a (Å)	29.526(5)
b (Å)	29.526(5)
c (Å)	6.0428(12)
α (deg)	90
β (deg)	90
γ (deg)	90
V (Å^3)	5268.2(17)
temperature (K)	298
Z	8
ρ_{calc} (g cm^{-3})	1.40
2θ range (deg)	4.000 – 37.000
R_{wp} (%)	6.28
R_p (%)	4.70
R_e (%)	6.64
S	0.9397

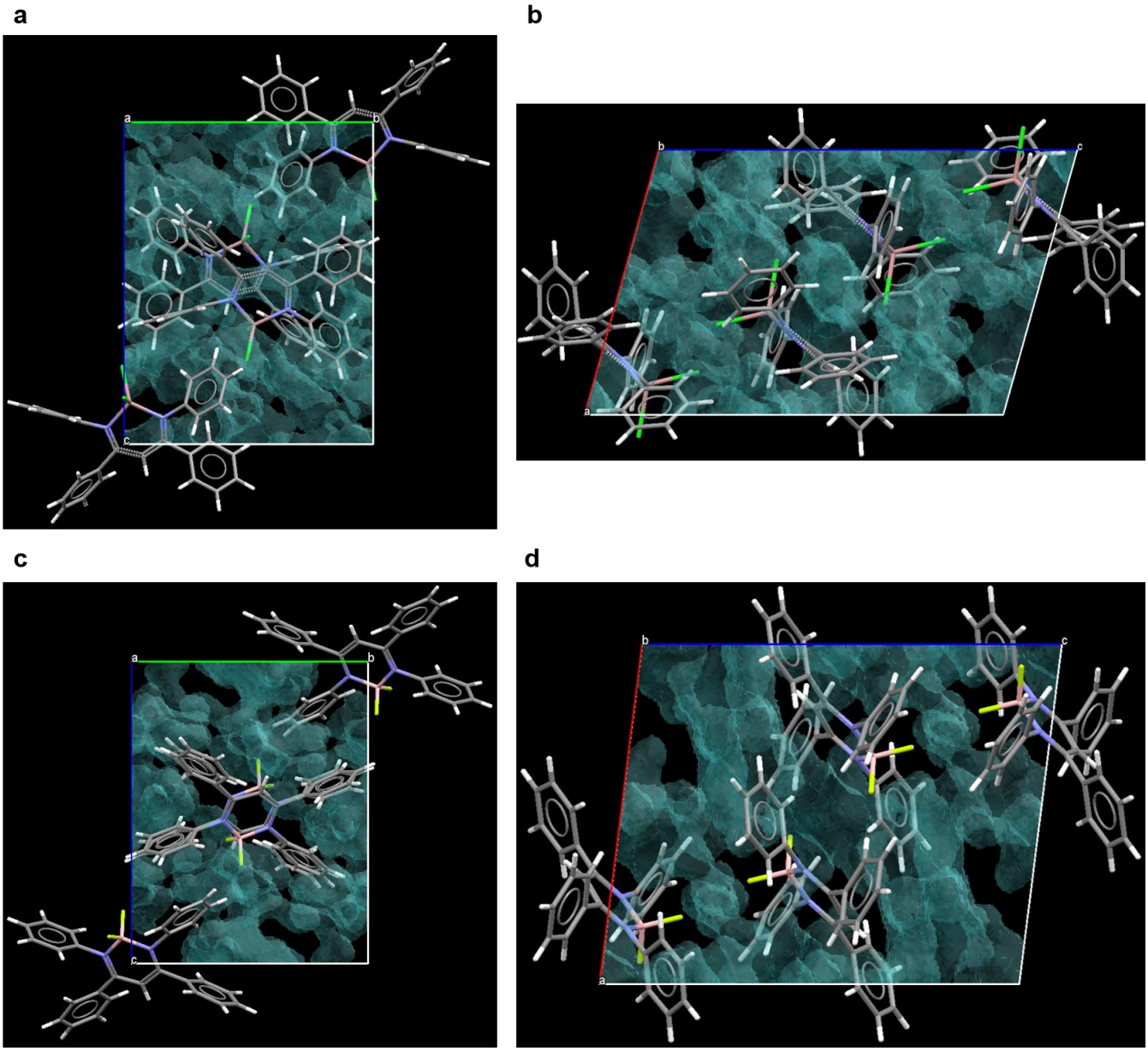

Figure S35. The crystal structures of gallium and borom diiminates. Voids in the unit cells are displayed as a transparent blue robe. Gallium complex along (a) *a*-axis and (b) *b*-axis. Boron complex along (a) *a*-axis and (b) *b*-axis.

Table S16. Fractions of the void volumes in the unit cell volumes of gallium and boron complexes

	gallium complex	boron complex
Volume of the unit cell ($Å^3$)	2411.99(5)	2138.07(5)
Volume of void ($Å^3$) [a]	546.33	405.51
Fraction (%) [a]	22.7	19.0

[a] Calculated with the program in the analytical package Mercury 3.6 by using the following parameters; probe radius = 0.5 Å and approx. grid spacing = 0.1 Å.

References

1) Yoshii, R.; Hirose, A.; Tanaka, K.; Chujo, Y. *Chem.–Eur. J.* **2014**, *20*, 8320−8324.

2) Kubelka, P.; Munk, F. *Z. Tech. Physik* **1931**, *12*, 593−601.

3) Daubert, T.E.; R.P. Danner. Physical and Thermodynamic Properties of Pure Chemicals Data Compilation. Washington, D.C.: Taylor and Francis, 1989.

4) Boultif, A.; Louer, D. *J. Appl. Cryst.* **2004**, *37*, 724−731.

5) Visser, J. W. *J. Appl. Cryst.* **1969**, *2*, 89−95.